Transnational University Limburg is a unique collaboration of two universities in two countries: the University of Hasselt and Maastricht University.

UHASSELT
KNOWLEDGE IN ACTION

www.uhasselt.be
Universiteit Hasselt
Campus Hasselt:
Martelarenlaan 42 | 3500 Hasselt
Campus Diepenbeek:
Agoralaan Gebouw D | 3590 Diepenbeek

UHASSELT
KNOWLEDGE IN ACTION

Maastricht University

Faculty of Medicine and Life Sciences
School for Life Sciences

Master of Biomedical Sciences

Masterthesis

Microglia-specific ADAM17 deficiency improves functional recovery after spinal cord injury

Inge Corstjens

Thesis presented in fulfillment of the requirements for the degree of Master of Biomedical Sciences, specialization Clinical Molecular Sciences

SUPERVISOR :

Prof. dr. Sven HENDRIX

MENTOR :

Mevrouw Daniela SOMMER

2017
2018

UHASSELT
KNOWLEDGE IN ACTION

Maastricht University

Faculty of Medicine and Life Sciences
School for Life Sciences
Master of Biomedical Sciences

Masterthesis

Microglia-specific ADAM17 deficiency improves functional recovery after spinal cord injury

Inge Corstjens

Thesis presented in fulfillment of the requirements for the degree of Master of Biomedical Sciences, specialization Clinical Molecular Sciences

SUPERVISOR :

Prof. dr. Sven HENDRIX

MENTOR :

Mevrouw Daniela SOMMER

Table of contents

Acknowledgements

During the past 8 months, I performed my senior internship in the Morphology group at BIOMED which resulted in this master thesis. However, the making of this thesis would not have been possible without the help and support of several people.

First of all, I would like to thank my promotor Prof. dr. Sven Hendrix for giving me the opportunity to perform my senior practical training in his research group. During this internship, he stimulated me to think critically about my research which will be a valuable skill for my future scientific career. Another word of appreciation goes to my daily supervisor Daniela Sommer for teaching my several new lab techniques and for revising my thesis. She gave me the responsibility to plan my own experiments and work independently in the lab which prepared me for my future career. I am very grateful for her guidance, support and help during this internship. Next, I would also like to thank the other members of the Morphology group (Stefanie Lemmens, Selien Sanchez, Céline Erens, Jana van Broeckhoven and Leen Timmermans) for welcoming me into their research group and for their help whenever necessary.

Furthermore, I would also like to thank my second examiner dr. Ronald Driesen for his time to discuss the progress of my project during our progress meeting.

Another word of appreciation goes to my fellow senior students at BIOMED for their support, help and advice during the past 8 months. Last but not least, I would also like to thank my parents for their continuous support, encouragements and their believe in me during this internship and my education.

List of abbreviations

5-HT	5-hydroxytryptamine
ADAM17	'a disintegrin and metalloproteinase 17'
ADAM17$^{ex/ex}$	hypomorphic ADAM17
ADAM17$^{wt/wt}$	wild-type ADAM17
Arg-1	Arginase-1
BMDM	bone marrow-derived macrophage
BMS	Basso Mouse Scale
CCR2	chemokine (C-C motif) receptor 2
CD	cluster of differentiation
CNS	central nervous system
CXCL1	chemokine (C-X-C motif) ligand 1
DAPI	4',6-diamidino-2-phenylindole
DMEM	Dulbecco's modified Eagle's medium
DMSO	dimethyl sulfoxide
dpi	days post-injury
ECM	extracellular matrix
EGFR	epidermal growth factor-receptor
ER	endoplasmic reticulum
FCS	fetal calf serum
GAPDH	glyceraldehyde 3-phosphate dehydrogenase
GFAP	glial fibrillary acidic protein
HMBS	hydroxymethylbilane synthase
Iba-1	ionized calcium-binding adapter molecule 1
ICAM-1	intercellular adhesion molecule-1
IFN-γ	interferon-γ
IL	interleukin
IL-R	interleukin receptor
iRhom	inactive homologues of rhomboid proteases
LCM	L929-conditioned medium
LPS	lipopolysaccharide
MBP	myelin basic protein
MerTK	Mer tyrosine kinase
MHC-II	major histocompatibility complex-II
PBS	phosphate-buffered saline
PFA	paraformaldehyde
PVDF	polyvinylidene difluoride
qPCR	quantitative polymerase chain reaction
RT	room temperature
SCI	spinal cord injury
SDS	sodium dodecyl sulfate
SEM	standard error of the mean
TBS	Tris-buffered saline
TGF	transforming growth factor
TMEM119	transmembrane protein 119
TNF-R	tumor necrosis factor-α receptor
TNF-α	tumor necrosis factor-α
TREM2	triggering receptor expressed on myeloid cells 2

Summary

Introduction: Spinal cord injury (SCI) affects each year between 250,000 and 500,000 people worldwide. Since the current treatment options for SCI are insufficient, further research on the complex SCI pathophysiology is necessary to identify more effective therapies. After SCI, an excessive inflammatory reaction is provoked, which is considered a major contributor to secondary damage. Resident microglia and monocyte-derived macrophages play an important role during inflammation through the release of inflammatory mediators and by phagocytosing cellular debris. The involvement of the enzyme 'a disintegrin and metalloproteinase 17' (ADAM17) in shedding, among others, inflammatory mediators and phagocytic receptors makes this enzyme an interesting target to modulate inflammation and phagocytosis after SCI. We therefore hypothesized that ADAM17 deficiency favors an anti-inflammatory environment by reducing the shedding of inflammatory mediators and by enhancing the resolution of inflammation through phagocytosis leading to an improved functional recovery after SCI.

Methods: The effect of ADAM17 after SCI was investigated by the induction of a T-cut hemisection in hypomorphic ADAM17 ($ADAM17^{ex/ex}$) mice, mice treated with a pharmacological ADAM17 inhibitor or microglia-specific ADAM17 knockout ($ADAM17flox^{+/+}$-$Cx3Cr1\text{-}Cre^{+/-}$) mice. Functional recovery of these mice was evaluated for 28 days using the Basso Mouse Scale. Furthermore, the spinal cords were isolated and analyzed on histological level. Besides, gene and protein expression of various inflammatory mediators and phagocytic receptors were determined in spinal cord tissue of $ADAM17^{ex/ex}$ and wild-type ($ADAM17^{wt/wt}$) mice. Finally, the effect of ADAM17 on the *in vitro* phagocytic capacity of bone marrow-derived macrophages (BMDMs) and primary microglia isolated from $ADAM17^{ex/ex}$ and $ADAM17^{wt/wt}$ mice was investigated.

Results: Our results show that ADAM17 deficiency as well as pharmacological ADAM17 inhibition leads to an improved functional recovery after SCI. In microglia-specific ADAM17 knockout mice a better functional recovery after SCI was also observed. Histological analysis revealed a significantly decreased number of $MHC\text{-}II^{+}$ cells in these mouse models, while an increased number of $5\text{-}HT^{+}$ fibers caudal to the lesion was observed in $ADAM17^{ex/ex}$ and $ADAM17flox^{+/+}$-$Cx3Cr1\text{-}Cre^{+/-}$ mice. Furthermore, an increased expression of various phagocytic receptors was observed in spinal cord tissue of $ADAM17^{ex/ex}$ mice after SCI. *In vitro* ADAM17 deficient BMDMs showed a significantly impaired phagocytic capacity of latex beads but a significantly improved phagocytic capacity of apoptotic neurons. A significantly improved phagocytic capacity of latex beads by ADAM17 deficient microglia was observed.

Conclusion: In conclusion, this study provides evidence that ADAM17 and more specifically microglial ADAM17 plays an important role in functional recovery after SCI. Our results suggest that the effect of ADAM17 deficiency on functional recovery is mediated by a reduced pro-inflammatory environment in the spinal cord. Furthermore, we also demonstrate that ADAM17 deficiency affects the *in vitro* phagocytic capacity of BMDMs and primary microglia. Based on our findings, ADAM17 seems to be a potential therapeutic target to improve functional recovery after SCI.

Keywords: Spinal cord injury, ADAM17, inflammation, phagocytosis and functional recovery.

1. Introduction

1.1. Spinal cord injury

Spinal cord injury (SCI) is defined as damage to the spinal cord that results in either temporary or permanent changes in motor, sensory or autonomic function below the level of injury (1). SCI patients usually suffer from permanent and devastating neurologic deficits and disability. Since SCI not only influences the physical health of patients but also their social and economic situation, it leads to a reduction in the patients' quality of life (1, 2). According to the World Health Organization, between 250,000 and 500,000 people worldwide are affected by an SCI each year (3). SCI is most prevalent in men (79.8%) and it mainly affects young adults between the age of 15 and 29 (1, 4). The major causes of SCI are road traffic accidents, falls, violence and sports (1, 3). The current treatment options for SCI such as surgical decompression, neuroprotective agents (e.g. immunosuppressant drugs) and rehabilitation are insufficient and only lead to a limited functional recovery after SCI (2, 5). Therefore, further research on the complex SCI pathophysiology is necessary to identify more effective therapies.

1.1.1. Spinal cord injury pathogenesis

SCI pathogenesis is divided into primary and secondary injury processes. Primary damage is initiated by a mechanical trauma such as a fractured or displaced vertebral column causing compression of the spinal cord. This results in axon disruption, damaged blood vessels causing micro-hemorrhages and broken neural cell membranes leading to neuronal degeneration at the lesion site (6). Primary damage is followed by a cascade of secondary damage processes including inflammation, oxidative stress, glutamate excitotoxicity, apoptosis, demyelination of surviving axons and glial scar formation (figure 1). Secondary injury is initiated immediately after SCI, persists for several weeks to months and contributes to the further expansion of the initial lesion (7-9). In the acute and subacute phases of SCI, a glial scar is formed in the perilesional area limiting secondary damage. This glial scar is characterized by the activation of astrocytes, so-called astrogliosis, leading to astrocyte proliferation, hypertrophy, an increased complexity of their processes and an increased glial fibrillary acidic protein (GFAP) expression. Later on, this scar forms a barrier against axon regeneration by the release of chondroitin sulfate proteoglycans and extracellular matrix (ECM) components (4, 10, 11).

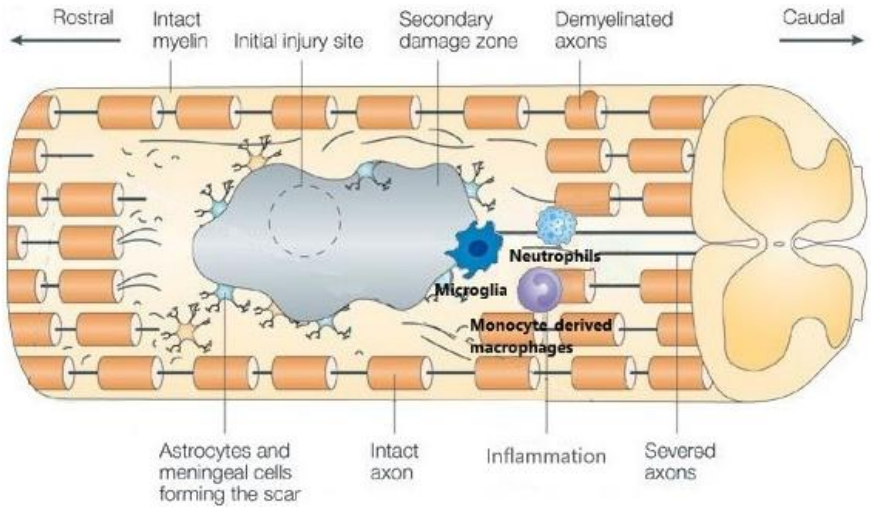

Figure 1: SCI pathogenesis. SCI is divided into primary and secondary damage processes. Primary damage, initiated by a mechanical trauma, leads to compression of the spinal cord which results in axon disruption, damaged blood vessels and broken neural cell membranes. The initial injury site is further expanded by a cascade of secondary damage processes including inflammation, demyelination of surviving axons and glial scar formation (Modified from (12)). *SCI, spinal cord injury.*

1.1.2. Inflammatory phase after spinal cord injury

The inflammatory response elicited after SCI is considered the major contributor to secondary damage (8). Inflammation is induced by the release of pro-inflammatory mediators from reactive cells at the site of injury and this response is aggravated by blood-spinal cord barrier disruption caused by the initial mechanical trauma (8, 9, 13). Despite the dual role of inflammation after SCI, the injured spinal cord favors a strong pro-inflammatory response that damages healthy tissue and aggravates the primary injury. An increase in the anti-inflammatory response, necessary for the clearance of cellular debris preventing neuron regeneration, is therefore considered a potential therapeutic strategy after SCI (7, 8, 13, 14).

During inflammation, one of the first cells infiltrating the site of injury are neutrophils. Their infiltration peaks 24 hours post-injury (7, 13, 15). An important role in SCI inflammation is attributed to resident microglia and infiltrating monocyte-derived macrophages. During the first 3 days after SCI, microglia are important, among others, for the clearance of tissue debris at the lesion site (14, 16). The immediate release of pro-inflammatory cytokines such as monocyte chemoattractant protein, interleukin-1β (IL-1β) and tumor necrosis factor-α (TNF-α) by microglia contributes to monocyte-derived macrophage infiltration from the peripheral circulation to the site of injury starting 2 to 3 days post-injury (dpi) (14, 16). Monocyte-derived macrophages start phagocytosing cellular debris after their infiltration into the lesion epicenter. Greenhalgh *et al.* observed the presence of monocyte-derived macrophages at the lesion epicenter for at least 42 dpi (16). Resident microglia resume their function of surveying the micro-environment by forming a border around the lesion. It is assumed that microglia thereby seal the lesion and prevent further damage (8, 14, 16, 17). During the first week after SCI, the less prevalent T cells also start infiltrating the site of injury (18). The role of T cells in SCI is controversial. On the one hand, they are essential for macrophage activation and they have the ability to recognize specific antigens such as myelin basic protein (MBP) leading

to axon demyelination and subsequent aggravation of the injury (7, 9, 18). On the other hand, a protective role is also attributed to T cells by the secretion of neuroprotective factors (19). T cells persists at the lesion site for months after injury (9, 18).

1.1.3. Resident microglia and monocyte-derived macrophages after spinal cord injury

Microglia, the resident immune cells of the central nervous system (CNS), respond immediately after SCI since microglia processes are constantly surveying the micro-environment for changes in homeostatic conditions. From day 2 to 3 post-injury, macrophages of myeloid origin, the monocyte-derived macrophages, are recruited to the injured spinal cord from the peripheral circulation (14, 16). Both resident microglia and monocyte-derived macrophages are professional phagocytes which play an important role in clearing cellular debris (14). Once activated, both cell types show similarities in morphology, gene expression and the expression of cell surface markers. Therefore, it is currently hardly possible to distinguish them (8).

Both resident microglia and monocyte-derived macrophages are highly plastic cells. Especially monocyte-derived macrophages are *in vitro* often classified into different activation states, the so-called M1/M2 phenotype. These phenotypes are *in vitro* distinguishable by the expression of cell surface markers, secreted molecules and intracellular enzymes (8). M1 (or classically activated) macrophages are activated by interferon-γ (IFN-γ) and via toll-like receptor activation. M1 macrophages are characterized by the production and release of various pro-inflammatory (including TNF-α, IL-1β, IL-6 and IFN-γ) and cytotoxic mediators (such as reactive oxygen species and reactive nitrogen species) (8, 14, 20). These mediators contribute to additional damage at the site of injury by killing neurons and glial cells (8, 21). M2 (also known as alternatively activated) macrophages are activated by IL-4 and IL-13 (14). M2 macrophages promote an anti-inflammatory response by the production and secretion of anti-inflammatory cytokines (such as IL-10 and IL-4), the secretion of growth factors (as transforming growth factor-β (TGF-β)) and the upregulation of ECM components and phagocytic receptors (14, 21). The M2 response leads to suppression of the inflammatory reaction and promotes repair and remodeling processes of injured tissue. However, an excessive or prolonged anti-inflammatory reaction eventually leads to fibrosis and scar formation, which is detrimental for axon regeneration (8, 14, 21).

Polarization towards either an M1 or an M2 phenotype is determined by both the micro-environment of the CNS and the type of material phagocytosed by these cells, such as myelin, apoptotic neutrophils or red blood cells (14, 16, 22). The injured spinal cord favors M1 polarization, since the M1 phenotype is predominant during SCI inflammation while only a small amount of the M2 phenotype is observed in the first week following SCI (8, 14, 20). A shift in the ratio between the M1 and M2 phenotype is therefore considered a promising strategy to improve functional recovery after SCI (8, 14).

1.2. 'A disintegrin and metalloproteinase 17' – "The enzyme that does it all"

Excessive inflammation after SCI is characterized by an upregulation of pro-inflammatory cytokines such as TNF-α. While membrane-bound TNF-α exerts its anti-inflammatory properties via TNF-α receptor II (TNF-RII), soluble TNF-α acts mainly via TNF-RI and leads to apoptosis and cell death (23-25). Soluble TNF-α is released after its cleavage by 'a disintegrin and metalloproteinase 17' (ADAM17), also known as TNF-α converting enzyme, which belongs to the ADAM protein family of type I transmembrane proteins (24-26).

1.2.1. Function of ADAM17

ADAM17 is a membrane-bound enzyme broadly expressed on most cells and tissues (24, 26). The function of ADAM17 is the cleavage, so-called shedding, and thereby release of ectodomains from more than 80 different transmembrane proteins. A variety of substrates are processed by ADAM17 including the cytokine TNF-α, cytokine receptors (such as IL-6 receptor (IL-6R), IL-1R and TNF-R), ligands of the epidermal growth factor-receptor (EGFR) (e.g. ErbB), the phagocytic receptor cluster of differentiation 36 (CD36) and cell adhesion proteins (as for instance intercellular adhesion molecule-1 (ICAM-1) and L-selectin) (24, 26). ADAM17-mediated shedding of a substrate results in the (in)activation or modulation of its function. Through this ectodomain shedding, ADAM17 influences intra- and extracellular signaling pathways as well as local and systemic reactions (25, 26).

The processing of this large variety of substrates by ADAM17 implies its involvement in the regulation of a plethora of body functions, developmental processes and diseases as for instance atherosclerosis and cancer (24, 26, 27). Due to the indispensable role of ADAM17 during development (24), ADAM17 deficient mice turned out to be not viable. These mice showed a severe dysregulation of epithelial development leading to defects in the development of skin, hair, cornea and several organs (26, 28). In contrast to mice, humans appear to have a compensation mechanism for a deficiency in functional ADAM17. This was observed in a study by Blaydon *et al.* where they identified a loss-of-function mutation in the ADAM17 gene as the cause of inflammatory skin and bowel disease while the patients developed normally until the age of 12 or remained healthy (29).

1.2.2. The structure of ADAM17

ADAM17 consists of several conserved protein domains: an N-terminal signal sequence is followed by a prodomain, the metalloproteinase or catalytic domain, a disintegrin domain, a cysteine-rich domain, a transmembrane domain and a cytoplasmic domain (figure 2) (24, 26).

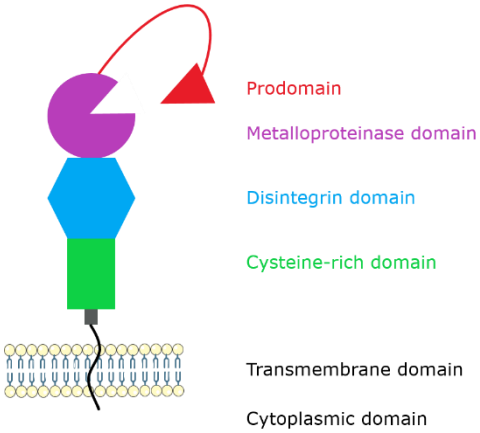

Figure 2: Structure of ADAM17. ADAM17 consists of an N-terminal signal sequence followed by a prodomain, the metalloproteinase domain, a disintegrin domain, a cysteine-rich domain, a transmembrane domain and a cytoplasmic domain (24, 26). *ADAM17, 'a disintegrin and metalloproteinase 17'.*

The ADAM17 prodomain acts as an inhibitor of ADAM17 activation and as a chaperone, protecting the enzyme from degradation during transport through the secretory pathway. The metalloproteinase or catalytic domain of ADAM17 is responsible for the shedding of membrane-bound proteins and contains the classical Zn^{2+} chelating sequence. ADAM17 is tightly regulated by its endogenous inhibitor, tissue inhibitor of metalloproteinase-3, which binds to the catalytic domain of ADAM17 and thus prevents shedding (23, 26). ADAM17 catalytic activity is also regulated by the interaction between its disintegrin domain and integrins. This interaction may lead to conformational changes so that ADAM17 substrates are either accessible or inaccessible for ADAM17 shedding (23, 26). The regulatory cysteine-rich domain or membrane proximal domain, followed by a highly conserved CANDIS domain, has an important role in the recognition of particular substrates and the activation of ADAM17 (24, 26). Hitherto, no consensus sequence elements were identified at the cleavage site of the large variety of ADAM17 substrates. Therefore, it is still unknown how ADAM17 recognizes its various substrates (25, 26). The ADAM17 cytoplasmic domain is involved in important signaling functions due to its binding to a variety of intracellular signaling molecules, as for instance protein kinase C, mitogen-activated protein kinase and extracellular signal-regulated kinase. The phosphorylation of the cytoplasmic tail regulates ADAM17 activity (23-26).

1.2.3. Maturation and activation of ADAM17

The catalytically inactive precursor of ADAM17 is synthesized in the endoplasmic reticulum (ER). Binding of the inactive ADAM17 precursor to inactive homologues of rhomboid proteases (iRhom) is required for their transport from the ER to the plasma membrane, an essential step during ADAM17 maturation. iRhom2, mainly located in the ER, is predominantly expressed in myeloid cells and microglia (24, 27, 30). iRhom1 is, particularly in the brain, also involved in this process (24, 27). Recently, Grieve *et al.* and Cavadas *et al.* showed that the interaction between iRhom2 and ADAM17 at the plasma membrane is essential for ADAM17 stabilization and prevention of lysosomal degradation. This complex inhibits ADAM17 activity, while its dissociation causes ADAM17 activation and subsequent shedding of ADAM17 substrates (31, 32). After the transport of ADAM17 in the trans-Golgi network by iRhom1/2, the pro-protein convertase furin cleaves the ADAM17 prodomain.

The mature form of ADAM17 is then transported from the late Golgi complex to the cell surface (figure 3), where it starts shedding ADAM17 substrates (24-26, 30).

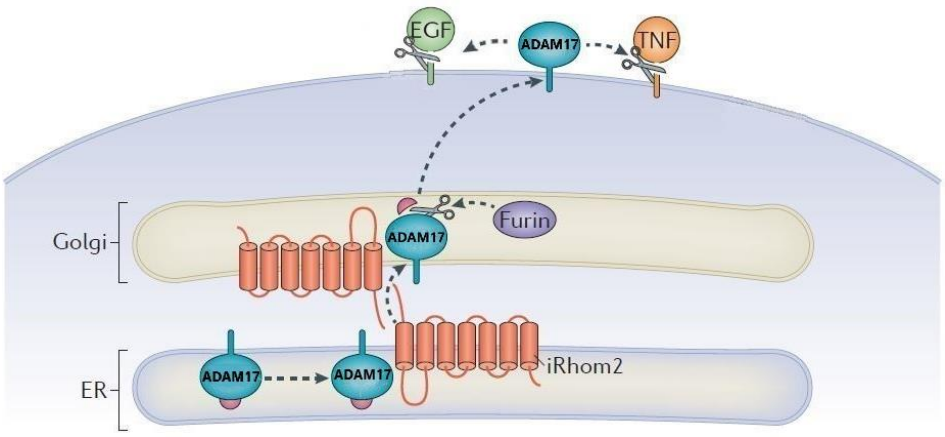

Figure 3: Maturation and activation of ADAM17. The catalytically inactive precursor of ADAM17 is synthesized in the ER. Binding of iRhom1/2 to ADAM17 is necessary for the transport of ADAM17 from the ER to the plasma membrane and ADAM17 maturation. The transport of ADAM17 to the trans-Golgi network causes ADAM17 maturation because of ADAM17 prodomain cleaving by the pro-protein convertase furin (modified from (30)). *ADAM17, 'a disintegrin and metalloproteinase 17'; ER, endoplasmic reticulum; iRhom1/2, inactive homologues of rhomboid proteases 1/2.*

1.2.4. The effect of ADAM17 on phagocytosis

As mentioned before, ADAM17 processes a large variety of substrates. Therefore, ADAM17 does not only have an effect on inflammation but also on the resolution of inflammation through e.g. phagocytosis. This influence is shown by the shedding of several phagocytic receptors such as CD36 and Mer tyrosine kinase (MerTK) receptor. Driscoll *et al.* observed that *in vivo* efferocytosis, the engulfment and degradation of apoptotic cells, and its subsequent anti-inflammatory effects are enhanced by macrophage ADAM17 deletion in a model of peritonitis. This effect appears to be mediated by the prevented cleavage and the elevated surface levels of the ADAM17 substrate CD36. This study indicates the involvement of ADAM17 in the resolution of inflammation by regulating the phagocytosis of, among others, apoptotic cells (33).

1.3. The role of ADAM17 in spinal cord injury

The shedding of a plethora of substrates by ADAM17 shows its role in regulating various body functions and diseases such as inflammation-mediated pathologies or cancer (24, 26, 27). During SCI, the inflammatory micro-environment of the injured spinal cord favors polarization of resident microglia and monocyte-derived macrophages towards the pro-inflammatory M1 phenotype (8, 14, 16, 20). Therefore, changes in this inflammatory micro-environment are considered to be a potential strategy to induce a shift in the ratio between the M1 and M2 phenotype (8, 14).

The involvement of ADAM17 in shedding various mediators of inflammation such as the pro-inflammatory cytokine TNF-α, cytokine receptors (TNF-R and IL-6R) and adhesion molecules (ICAM-1 and L-selectin) makes this enzyme an interesting and promising target to modulate inflammation

(24, 26). During SCI, phagocytosis of cellular debris by resident microglia and monocyte-derived macrophages plays an important role in diminishing inflammation and in initiating repair processes. As observed in the study of Kroner *et al.*, myelin phagocytosis induces *in vitro* a phenotypic shift from an M1 to an M2 phenotype. However, this shift fails to occur in the injured spinal cord probably due to the highly pro-inflammatory micro-environment (14, 34). The role of ADAM17 in shedding various phagocytic receptors gives this enzyme potential in modulating phagocytic activity of for instance resident microglia and monocyte-derived macrophages. The effect of ADAM17 on phagocytosis is already shown in the study by Driscoll *et al.*, as mentioned before (33).

Previous research studying the effect of ADAM17 inhibition in a SCI mouse model showed the involvement of ADAM17 during SCI. Besides, it was shown that ADAM17 signaling was necessary for microglial survival *in vitro* (35). To investigate the role of ADAM17, hypomorphic ADAM17 ($ADAM17^{ex/ex}$) mice were generated with an almost complete absence of functional ADAM17 protein in the whole organism. These mice were created by the induction of a new artificial exon which starts with a premature translational stop codon in the ADAM17 gene, called the exon induced translational stop strategy. $ADAM17^{ex/ex}$ mice are viable and show due to the importance of ADAM17 during developmental processes for instance eye, hair and skin defects. Since ADAM17 is ubiquitously expressed, it is essential to design cell and tissue-specific strategies to target ADAM17. Therefore, conditional and inducible ADAM17 knockout animals were generated to study the cell and tissue-specific roles of ADAM17 (23, 26, 28). These various mouse models are used to unravel the precise mechanisms of ADAM17 involvement in functional recovery after SCI.

1.4. Aims of the study

The aim of this research is to elucidate the mechanisms behind the effect of ADAM17 on SCI, especially on inflammation and phagocytosis. ADAM17 involvement in shedding various inflammatory mediators and phagocytic receptors makes this enzyme an interesting target to modulate the inflammatory response and phagocytic activity of professional phagocytes (24, 26). In this study, we hypothesized that ADAM17 deficiency favors an anti-inflammatory environment by reducing the shedding of inflammatory mediators and by enhancing the resolution of inflammation through phagocytosis leading to an improved functional recovery after SCI (figure 4). First, we investigated the effect of ADAM17 on functional recovery after SCI using $ADAM17^{ex/ex}$ mice and by inhibiting ADAM17 via a pharmacological inhibitor. In a second part of the project, a tamoxifen-inducible microglia-specific ADAM17 knockout ($ADAM17flox^{+/+}$-Cx3Cr1-CreERT2) mouse model was used to study the effect of ADAM17 on microglia and to determine the role of microglial ADAM17 on the functional recovery after SCI. Furthermore, *in vitro* the phagocytic capacity of bone marrow-derived macrophages (BMDMs) and primary microglia isolated from $ADAM17^{ex/ex}$ and wild-type ($ADAM17^{wt/wt}$) mice was investigated.

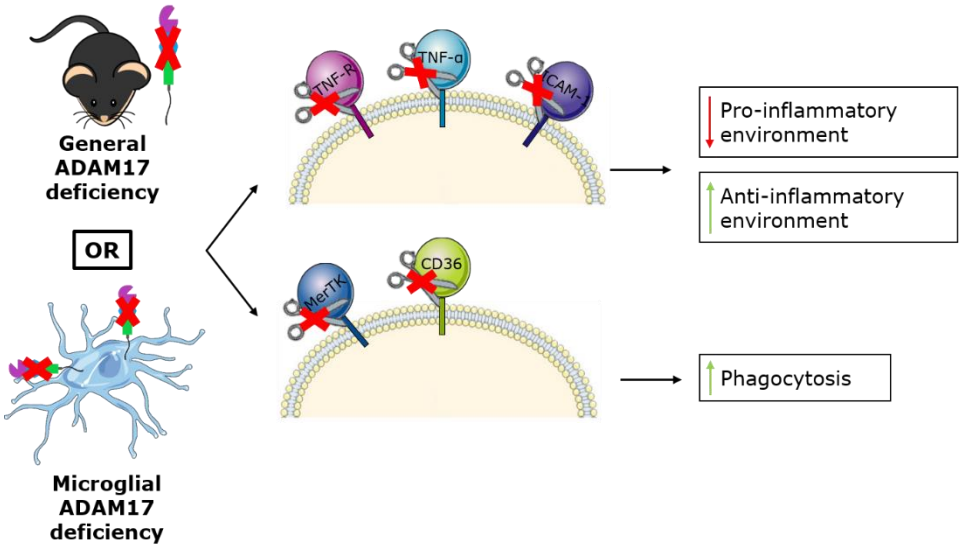

Figure 4: ADAM17 deficiency promotes an anti-inflammatory environment and phagocytosis after SCI. In this study, we hypothesized that ADAM17 deficiency favors an anti-inflammatory environment by the reduced production of soluble TNF-α and by enhancing the resolution of inflammation through phagocytosis, which leads to an improved functional recovery after SCI. The deficiency of ADAM17 promotes an anti-inflammatory environment in the injured spinal cord, because of the impeded shedding of various mediators of inflammation such as TNF-α, TNF-R and ICAM-1. ADAM17 deficiency not only has an effect on the inflammatory response following SCI but also on the phagocytic capacity of resident microglia and monocyte-derived macrophages. The inhibited shedding of various phagocytic receptors, including CD36 and MerTK, improves their phagocytic capacity and thereby the resolution of inflammation and inhibitory factors necessary for regeneration. *ADAM17, 'a disintegrin and metalloproteinase 17'; SCI, spinal cord injury; TNF-α, tumor necrosis factor-α; TNF-R, tumor necrosis factor-receptor; ICAM-1, intercellular adhesion molecule-1; CD36, cluster of differentiation 36; MerTK, Mer tyrosine kinase.*

2. Materials and methods

2.1. Animals

ADAM17$^{ex/ex}$ and ADAM17$^{wt/wt}$ mice were used for *in vivo* and *in vitro* experiments. Heterozygous ADAM17$^{wt/ex}$ breeding mice were kindly provided by Prof. Dr. Stefan Rose-John and Dr. Athena Chalaris-Rißmann (Christian-Albrechts University, Kiel, Germany). As previously reported, ADAM17$^{ex/ex}$ mice show eye, hair and skin defects (28), therefore *in vivo* experiments could not be performed blinded.

For the inhibitor experiment, 10-week old female C57BL/6J mice (Janvier, Le Genest Saint Isle, France) were used. Animals were distributed equally among the groups according to their Basso Mouse Scale (BMS) score right after surgery. These mice received an intraperitoneal injection of an ADAM10/17 inhibitor (GW280264x, Aobious Inc., Gloucester, Massachusetts, USA), a specific ADAM10 inhibitor (GI254023x, Sigma-Aldrich, Overijse, Belgium) or the vehicle every day for one week starting 4 hours post-surgery. GW280264x and GI254023x were dissolved in 0.6% dimethyl sulfoxide (DMSO) in phosphate-buffered saline (PBS) at a concentration of 100 µg/kg.

Mice expressing tamoxifen-inducible Cre-recombinase under the Cx3Cr1 promotor (Cx3Cr1-CreERT2 mice), previously described by Prof. Dr. Steffen Jung (36), were bred with ADAM17flox$^{+/+}$ mice (strain 009597, Jackson Laboratory) for at least 2 generations to create ADAM17flox$^{+/+}$-Cx3Cr1-Cre mice. For the induction of the Cx3Cr1-driven Cre-recombinase, tamoxifen was administered twice to the mice via oral gavage (8 mg/ml tamoxifen (Sigma-Aldrich) dissolved in corn oil (Sigma-Aldrich) at a concentration of 20 mg/ml) every other day at the age of 4-5 weeks.

Mice were housed in a conventional animal facility at Hasselt University under standardized conditions, such as a 12h light-dark cycle, a temperature-controlled room (20 ± 3°C) and with food and water *ad libitum*. All experiments were approved by the local ethical committee of Hasselt University and were performed according to the guidelines described in Directive 2010/63/EU on the protection of animals used for scientific purposes.

2.2. Genotyping

The offspring of the heterozygous ADAM17$^{wt/ex}$ and ADAM17flox$^{+/+}$-Cx3Cr1-Cre$^{+/-}$ breeding couples were genotyped by the extraction of genomic DNA from ear punches using the Extracta™ DNA Prep for PCR tissue (Quanta Biosciences, Gaithersburg, Maryland, USA) according to the manufacturer's instructions. The PCR mixture (25 µl) contained 1x Kapa2G Fast (Sigma-Aldrich), 0.5 µM of forward and reverse primers (table S1) and genomic DNA. The obtained PCR product was separated by gel electrophoresis on a 2% agarose gel. At last, the gels were visualized using the Gel Doc™ XR+ system (Bio-Rad Laboratories, Temse, Belgium).

2.3. Isolation of microglia from adult mice

The efficiency of Cre-lox recombination was evaluated by the isolation of microglia from adult ADAM17flox$^{+/+}$-Cx3Cr1-Cre$^{+/-}$ and ADAM17flox$^{+/+}$-Cx3Cr1-Cre$^{-/-}$ mice. These mice first received an intraperitoneal injection of an anesthetic overdose (200 mg/kg Dolethal; Vetoquinol, Aartselaar,

Belgium) and were transcardially perfused with cold PBS containing heparin. The different steps in the protocol were performed at 4°C unless otherwise mentioned. Spinal cords and brains were isolated and dissociated using 175 U/ml collagenase dissolved in Hank's balanced salt solution containing Ca^{2+} and Mg^{++} for 1 hour at 37°C. Next, the dissociated tissue was centrifuged for 5 minutes at 400g and then washed with Dulbecco's modified Eagle's medium (DMEM; Sigma-Aldrich), 10% heat-inactivated fetal calf serum (FCS) and DNase (STEMCELL technologies, Grenoble, France). After 15 minutes incubation at room temperature (RT), the cell suspension was centrifuged for 5 minutes at 400g. The cell pellet was subsequently resuspended in 30% Percoll in 1x PBS and centrifuged for 10 minutes at 700g. The obtained layer of fat was removed and the cell pellet was resuspended in 1x PBS, containing 0.05 mg/ml DNase, which was incubated for 15 minutes at RT. After washing with MACS buffer (1x PBS with 0.5% bovine serum albumin and 2 mM ethylenediaminetetraacetic acid) for 5 minutes at 700g, the cell suspension was filtered through a 35 µm strainer and centrifuged for 5 minutes at 700g. Microglia were isolated using CD11b MicroBeads (Miltenyi Biotec, Leiden, The Netherlands) according to the manufacturer's instructions. Briefly, the cell pellet was resuspended in MACS buffer and CD11b MicroBeads and incubated for 15 minutes. The cells were washed with MACS buffer and centrifuged for 10 minutes at 700g and the cells were resuspended in MACS buffer. The $CD11b^+$ cells were magnetically separated by letting the cell suspension flow through the MACS columns of the MACS separator. Subsequently, $CD11b^+$ cells were collected and either used for RNA isolation using the RNeasy Mini Kit (Qiagen, Antwerp, Belgium) according to the manufacturer's instructions or resuspended in RIPA buffer (150 mM NaCl, 50 mM Tris base (pH = 8), 0.5% sodium deoxycholate, 0.1% sodium dodecyl sulfate (SDS) and 1% Triton X-100 supplemented with an EASYpack complete protease inhibitor cocktail tablet (Roche, Sigma-Aldrich)) for further use.

2.4. Experimental spinal cord injury

A T-cut hemisection injury was performed as previously described (37, 38). Briefly, 10- to 12-week old mice were anesthetized by 3% isoflurane (IsoFlo®, Zoetis Belgium SA, Zaventem, Belgium). The spinal cord was exposed by a partial laminectomy at thoracic level T8. Mice were subjected to a bilateral hemisection (T-cut hemisection) injury by the transection of the left and right dorsal funiculus, the dorsal horns and the ventral funiculus, using iridectomy scissors. This T-cut hemisection results in a complete transection of the dorsomedial and ventral corticospinal tract and induces impairment of several other descending and ascending tracts. Afterwards, muscles were sutured and the back skin was closed with wound clips (BD Autoclip®, BD biosciences, Erembodegem, Belgium). As a post-operative pain treatment, a subcutaneous injection of the analgesic Temgesic (0.1 mg/kg; Val d'Hony Verdifarm, Beringen-Paal, Belgium) was given close to the wounded area. Hypoglycemia and dehydration was avoided by an intraperitoneal injection of 20% glucose (Baxter, Lessen, Belgium) and, if necessary, eyes were remoistened with drops of NaCl. Subsequently, mice were placed in a temperature-controlled chamber (33°C) to avoid hypothermia and were placed back in their cages after they regained consciousness. Bladders were manually emptied every day until return of bladder function.

2.5. Locomotion tests

Functional recovery of the mice was scored for 28 days using the BMS test (39). BMS is a 10-point scale (9 = normal locomotion, 0 = complete hind limb paralysis) based on hind limb movements made in an open field during a 4-minute interval. Mice were scored daily during the first ten days after SCI surgery and every other day during the remaining period. Functional recovery was evaluated by an investigator blinded to the experimental groups.

2.6. Quantitative polymerase chain reaction

The efficiency of Cre-lox recombination was determined by measuring ADAM17 mRNA expression using quantitative polymerase chain reaction (qPCR) in microglia isolated from adult ADAM17flox$^{+/+}$-Cx3Cr1-Cre$^{+/-}$ and ADAM17flox$^{+/+}$-Cx3Cr1-Cre$^{-/-}$ mice. RNA was extracted from these microglia using the RNeasy Mini Kit (Qiagen) according to the manufacturer's instructions. Besides, gene expression was investigated at different time points post-injury (1, 3 and 7 dpi). Therefore, ADAM17$^{ex/ex}$ and ADAM17$^{wt/wt}$ mice were transcardially perfused with Ringer solution. Uninjured mice (without SCI) of both genotypes were included into the analysis as a control. Standardized areas of spinal cord tissue (5 mm cranial and 5 mm caudal to the lesion center) were collected. Total RNA was isolated from these spinal cords using the PARIS^{TM} kit (Thermo Fisher Scientific, Erembodegem, Belgium) according to the manufacturer's instructions with minor adaptations (37). The concentration and the purity of the RNA were determined using the NanoDrop Spectrophotometer (Thermo Fisher Scientific).

Next, cDNA was synthesized from 0.15 µg total RNA using the qScript cDNA SuperMix (1x) (Quanta Biosciences). Subsequently, a qPCR was performed by the StepOnePlus Real-Time PCR system, using universal cycling conditions (20 s at 95°C and 40 cycles of 3 s at 95°C and 30 s at 60°C) (Applied Biosystems, Gaasbeek, Belgium). The qPCR reaction mixture contained fast SYBR Green master mix (Applied Biosystems), 10 µM forward and reverse primers, MilliQ water and cDNA in a total reaction volume of 10 µl. Primer sequences are provided in table S2. Relative quantification of the gene expression was performed by the comparative $2^{-\Delta\Delta CT}$ method. The data was normalized to the most stable reference genes as previously described (40). GeNorm software identified hydroxymethylbilane synthase (HMBS) and glyceraldehyde 3-phosphate dehydrogenase (GAPDH) as the most stable reference genes.

2.7. Western blot analysis

The efficiency of Cre-lox recombination was determined by measuring ADAM17 protein expression in microglia isolated from adult ADAM17flox$^{+/+}$-Cx3Cr1-Cre$^{+/-}$ and ADAM17flox$^{+/+}$-Cx3Cr1-Cre$^{-/-}$ mice and resuspended in RIPA buffer. To investigate protein expression at different time points post-injury (1, 3, 7, 28 and 42 dpi), ADAM17$^{ex/ex}$ and ADAM17$^{wt/wt}$ mice were transcardially perfused with Ringer solution, as described before. Uninjured mice (without SCI) of both genotypes were included into the analysis as a control. Standardized areas of spinal cord tissue (5 mm cranial and 5 mm caudal to the lesion center) were collected and proteins were isolated using the PARIS^{TM} kit (Thermo Fisher Scientific) according to the manufacturer's instructions with minor adaptations (37). The

protein concentration was measured using the Pierce BCA Protein Assay Kit (Thermo Fisher Scientific) according to the manufacturer's instructions. At the end, the results were read at 570 nm with an iMark Microplate Absorbance Reader (Bio-Rad Technologies). Samples (20 µg of protein) were separated on a 7.5 or 12% SDS-polyacrylamide gel at 140V for 1.5 hour. Thereafter, the proteins were transferred from the gel to a polyvinylidene difluoride (PVDF) membrane (Merck Millipore, Overijse, Belgium) for 1.5 hours at 350 mA. The PVDF membrane was then blocked for at least 1 hour with 5% milk powder in 1x TBS-T (Tris-buffered saline (TBS) containing 0.1% Tween 20) and incubated overnight at 4°C with the primary antibody (diluted in 1x TBS-T with 0.02% sodium azide; table S3). After repeating washing steps with 1x TBS-T, the horse radish peroxidase-conjugated secondary antibody (diluted in 5% milk powder in 1x TBS-T; table S3) was applied for 1 hour at RT. The target protein was visualized by applying Pierce ECL Plus Western Blotting Substrate (Thermo Fisher Scientific) and with the use of the ImageQuant LAS 4000 mini (GE Healthcare, Diegem, Belgium). β-actin served as a loading control.

2.8. Immunohistochemistry

Mice received an intraperitoneal injection of an anesthetic overdose (200 mg/kg Dolethal; Vetoquinol) at 28 dpi. Subsequently, they were transcardially perfused with Ringer solution containing heparin followed by 4% paraformaldehyde (PFA) in PBS (pH = 7.4). Spinal cords were isolated and stored overnight in post-fixation solution (5% sucrose in 4% PFA) at 4°C followed by several days of cryoprotection in 30% sucrose in 1x PBS at 4°C. Afterwards, spinal cords were embedded in optimal cutting temperature compound (Leica, Diegem, Belgium) and frozen using liquid-nitrogen cooled isopentane. Next, 10 µm thick sagittal spinal cord sections were cut and immunohistochemical stainings were performed.

The spinal cord sections were first blocked in 10% protein block (Dako, Heverlee, Belgium) in 1x PBS for 1 hour at RT. Optionally, permeabilization was performed for 30 minutes using 10% protein block in 1x PBS containing 0.5% Triton X-100. The primary antibodies (table S4) were diluted in 1x PBS with 1% protein block and 0.05% Triton X-100 and incubated overnight at 4°C in a humidified chamber. After repeating washing steps with 1x PBS, secondary antibodies (table S4) were applied for 1 hour at RT in the dark. If the spinal cord sections were stained for Arginase-1 (Arg-1) and major histocompatibility complex-II (MHC-II), the following protocol was used. First, sections were permeabilized for 30 minutes using 0.1% Triton X-100 in TBS (pH 7.5) and blocked with 10% protein block in TBS for 1 hour at RT. Primary antibodies (table S4) were diluted in TBS containing 10% milk powder and incubated at 4°C in a humidified chamber. Following repeating washing steps with TBS, secondary antibodies (table S4) were applied for 1.5 hours at RT in the dark. The remaining steps of the protocol are equal for all stainings, after the removal of unbound antibodies, a 4',6-diamidino-2-phenylindole (DAPI) (Invitrogen, Erembodegem, Belgium) counterstaining was performed for 10 minutes and sections were mounted with fluorescent mounting medium (Dako). The specificity of the secondary antibodies was verified by including control stainings, in which the primary antibody was not applied. Images were taken with a Nikon Eclipse 80i microscope and a digital sight camera DS-2MBWc (Nikon, Brussels, Belgium).

2.9. Quantitative image analysis

Quantitative image analysis was performed on original unmodified images of spinal cord sections representing the lesion center, using the ImageJ open source software (National Institutes of Health, Bethesda, Maryland, USA). The lesion size and demyelinated area were evaluated by delineating the area without GFAP and MBP expression, respectively. Quantification of astrogliosis (GFAP expression) and microglia/macrophages infiltration (ionized calcium-binding adapter molecule 1 (Iba-1) expression) was performed in the perilesional area by intensity analysis, within square areas of 100 µm x 100 µm extending 600 µm cranial and 600 µm caudal from the lesion epicenter. The number of $CD4^+$ cells was quantified by counting them throughout the entire spinal cord, while the MHC-II^+, Arg-1^+ and transmembrane protein 119 $(TMEM119)^+$ cells were quantified by counting them at the lesion site and the perilesional area. The recovery of serotonergic neurons was evaluated by determining the ratio between the length of the 5-hydroxytryptamine $(5\text{-}HT)^+$ fibers caudal and cranial to the lesion epicenter.

2.10. Isolation and culturing of bone marrow-derived macrophages

$ADAM17^{ex/ex}$ and $ADAM17^{wt/wt}$ mice were euthanized by cervical dislocation. Bone marrow was isolated from the femur and tibia by flushing them with ice-cold PBS. The obtained cell suspension was cultured for 7-10 days in RPMI1640 medium (Lonza, Verviers, Belgium) supplemented with 10% heat-inactivated FCS, 1% penicillin/streptomycin and 15% L929-conditioned medium (LCM) containing macrophage colony-stimulating factor to ensure differentiation towards macrophages. Culture medium was changed approximately every 3 days. Cells were maintained at 37°C in a humidified incubator with an air atmosphere of 5% CO_2.

2.11. Isolation and culturing of primary microglia

Primary microglia cultures were prepared from postnatal P0-P3 pups of $ADAM17^{wt/wt}$ and $ADAM17^{ex/ex}$ mice (41). Briefly, isolated forebrains of mouse pups were incubated in L15 Leibovitz medium (Gibco, Thermo Fisher Scientific) with 1:10 Trypsin (Sigma-Aldrich) for 15 minutes at 37°C. Subsequently, the tissue was dissociated in DMEM high glucose medium supplemented with 10% FCS and 1% penicillin/streptomycin using a Pasteur pipette. The dissociated tissue was passed through a 70 µm cell strainer, rinsed with DMEM high glucose supplemented with 10% FCS and 1% penicillin/streptomycin and centrifuged at 1000 rpm for 10 minutes at RT. The cell suspension was seeded at 2 forebrains per T75 cell culture flask. After 2 days, the culture medium was refreshed. After reaching 80% confluency, 2/3 DMEM high glucose with 10% FCS and 1% penicillin/streptomycin containing 1/3 LCM was added. Microglia were isolated approximately 6 days later using the shake-off method (200 rpm, 2 hours, RT). Microglia were centrifuged at 1000 rpm for 10 minutes at RT and resuspended in 2/3 DMEM high glucose with 10% FCS, 1% penicillin/streptomycin and 1/3 LCM for further use in the phagocytosis assay. Cells were maintained at 37°C in a humidified incubator with an air atmosphere of 5% CO_2.

2.12. Culturing of Neuro-2a cells and induction of apoptosis

The Neuro-2a cell line is a murine neuroblast cell line purchased from American Type Culture Collection (CCL-131; ATCC, Molsheim Cedex, France). The cell line was cultured in DMEM high glucose medium supplemented with 10% heat-inactivated FCS and 1% penicillin/streptomycin. Neuro-2a cells were maintained at 37°C with 5% CO_2 in a humidified incubator.

Apoptotic Neuro-2a cells were generated by UV exposure at 254 nm for 15 minutes followed by an 1 hour incubation at 37°C in a 5% CO_2 atmosphere. Apoptosis/necrosis was determined by annexin V and propidium iodide staining using the apoptosis/necrosis detection kit (Abcam, Cambridge, United Kingdom).

2.13. Phagocytosis assay

BMDMs or microglia were seeded in a 24-well plate at a density of 2 x 10^5 cells per well in complete RPMI1640 medium supplemented with 15% LCM or 2/3 DMEM high glucose with 10% FCS, 1% penicillin/streptomycin and 1/3 LCM, respectively. After 24 hours, the BMDMs and microglia were treated with lipopolysaccharide (LPS, 200 ng/ml; PeproTech, London, United Kingdom), IFN-γ (100 ng/ml; PeproTech) or IL-4 (33 ng/ml; PeproTech). After overnight incubation, fluorescent red 0.2 µm latex beads (Sigma-Aldrich) or DiI labeled apoptotic Neuro-2a cells (ratio 4:1) were added to the medium of the cells. After an 1.5 hour incubation, the cells were washed several times with 1x PBS and collected in 350 µl FACS buffer (1x PBS supplemented with 2% FCS and 0.1% sodium azide). The amount of latex beads or DiI labeled apoptotic Neuro-2a cells phagocytosed was determined using FACS Fortessa (BD Biosciences).

2.14. Statistical analysis

GraphPad Prism 7 software (GraphPad Software, Inc., La Jolla, California, USA) was used to perform statistical analyses. The BMS locomotion tests and histological evaluation of astrogliosis and microglia/macrophages infiltration were analyzed using two-way ANOVA for repeated measurements with a Bonferroni *post hoc* test for multiple comparisons. All other differences between two groups were analyzed by the non-parametric Mann-Whitney U test. Multiple groups were compared by a Kruskal Wallis test followed by a Dunn's multiple comparisons test. Differences with a p-value of < 0.05 were considered statistically significant. Data in graphs are presented as mean ± standard error of the mean (SEM) or as mentioned otherwise.

3. Results

First, we investigated the effect of ADAM17 on functional recovery after SCI. To address this question, ADAM17$^{ex/ex}$ mice, which express reduced levels of ADAM17, or C57BL/6J mice treated with a pharmacological ADAM17 inhibitor were subjected to a T-cut hemisection. Functional recovery of these mice was evaluated using the BMS and their spinal cords were further analyzed on histological level. Besides, gene and protein expression levels of various inflammatory mediators and phagocytic receptors were determined in spinal cord tissue of ADAM17$^{ex/ex}$ and ADAM17$^{wt/wt}$ mice isolated at different time points post-injury. In a second part of the project, the role of microglial ADAM17 on functional recovery after SCI was studied using a tamoxifen-inducible microglia-specific ADAM17 knockout (ADAM17flox$^{+/+}$-Cx3Cr1-Cre$^{+/-}$) mouse model. The spinal cords of these mice were further evaluated on histological level. Finally, the effect of ADAM17 on the *in vitro* phagocytic capacity of BMDMs and primary microglia isolated from ADAM17$^{ex/ex}$ and ADAM17$^{wt/wt}$ mice was investigated.

3.1. ADAM17 deficiency leads to a better functional recovery after SCI

To investigate the effect of ADAM17 on the functional recovery after SCI, ADAM17$^{ex/ex}$ and ADAM17$^{wt/wt}$ mice were subjected to a T-cut hemisection at thoracic level T8. The functional recovery of these mice was assessed for 28 days using the BMS. BMS scores range from 0 (= no ankle movement) to 9 (= normal locomotion), for instance a score of 3 is plantar placing or dorsal stepping while a score of 4 is occasional plantar stepping (39). Locomotor recovery was significantly improved in ADAM17$^{ex/ex}$ mice from day 8 onwards ($p < 0.001$) compared to ADAM17$^{wt/wt}$ mice (figure 5). These results indicate that ADAM17 deficiency leads to a better functional recovery after SCI.

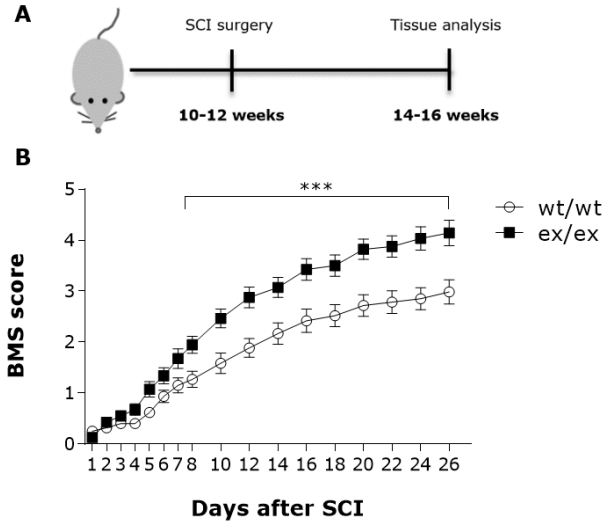

Figure 5: ADAM17 deficiency leads to a better functional recovery after SCI. A) 10- to 12-week old mice with a reduced ADAM17 expression in all tissues (ADAM17$^{ex/ex}$ mice, ex/ex, n = 28) and wild-type (ADAM17$^{wt/wt}$, wt/wt, n = 30) mice were subjected to a T-cut hemisection. Functional recovery was assessed for 28 days using the BMS where after these mice were sacrificed and their spinal cord tissue was analyzed. B) ADAM17$^{ex/ex}$ mice displayed an improved functional recovery from day 8 after SCI compared to ADAM17$^{wt/wt}$ mice. Data are presented as mean ± SEM. ***$p < 0.001$. *ADAM17, 'a disintegrin and metalloproteinase 17'; SCI, spinal cord injury; BMS, Basso Mouse Scale.*

3.2. ADAM17 deficiency affects myelination, serotonergic neuron recovery and the inflammatory response after SCI

Spinal cord tissue of ADAM17$^{ex/ex}$ and ADAM17$^{wt/wt}$ mice was isolated 28 dpi and further analyzed by immunohistochemistry. Demyelinated area, lesion size and astrogliosis (figure 6A-D) was analyzed by MBP and GFAP immunofluorescence. Measurement of the demyelinated area, the MBP-negative area, showed a significant increase ($p < 0.05$) in ADAM17$^{ex/ex}$ mice compared to ADAM17$^{wt/wt}$ mice (figure 6A-B). However, no significant difference in lesion size, defined as the GFAP-negative area, was observed between ADAM17$^{ex/ex}$ and ADAM17$^{wt/wt}$ mice (figure 6C). Furthermore, astrogliosis was determined by measuring GFAP intensity 600 µm caudal and 600 µm cranial from the lesion epicenter. No significant difference in astrogliosis was observed 28 dpi between ADAM17$^{ex/ex}$ and ADAM17$^{wt/wt}$ mice (figure 6D). Next, the recovery of serotonergic neurons was evaluated by determining the ratio between the length of the 5-HT$^+$ fibers caudal and cranial to the lesion epicenter. ADAM17$^{ex/ex}$ mice showed a significant increased 5-HT$^+$ fiber ratio ($p < 0.05$) compared to ADAM17$^{wt/wt}$ mice (figure 6E).

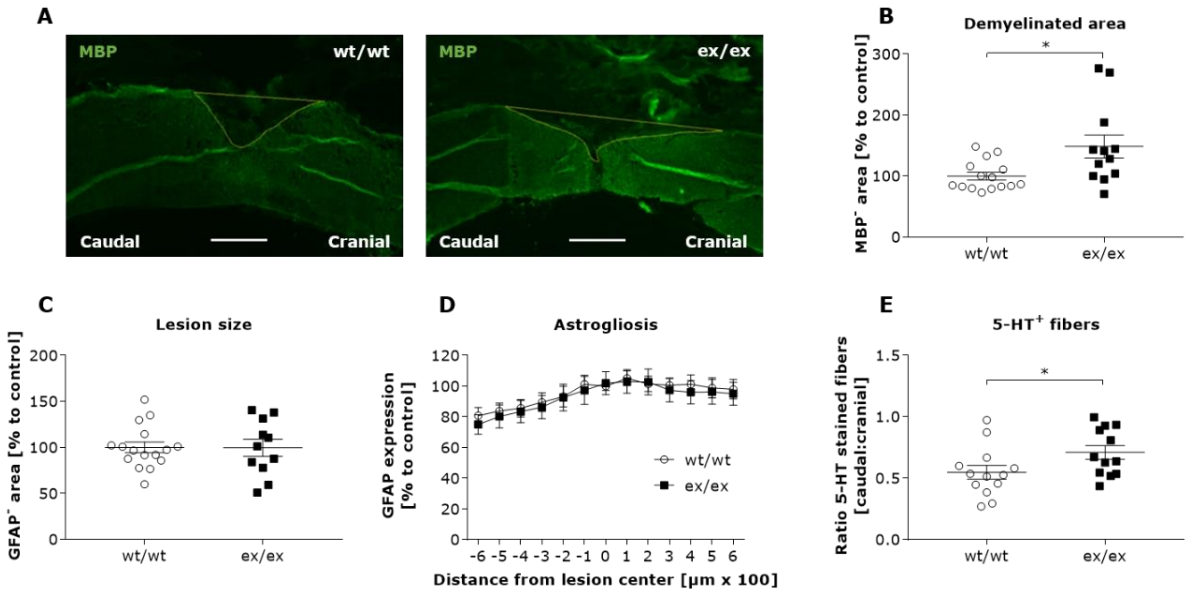

Figure 6: ADAM17 deficiency leads to an increased demyelinated area and a better recovery of serotonergic fibers. Spinal cord sections of ADAM17$^{ex/ex}$ (ex/ex, n = 11-13) and ADAM17$^{wt/wt}$ mice (wt/wt, n = 13-16) were further analyzed on histological level. A) Representative images of spinal cord sections, including the lesion epicenter, from ADAM17$^{ex/ex}$ and ADAM17$^{wt/wt}$ mice stained for MBP were used to measure the demyelinated area. Scale bar: 500 µm. B) ADAM17$^{ex/ex}$ mice showed a significant increased demyelinated area, the MBP-negative area, compared to ADAM17$^{wt/wt}$ mice. C) No difference in lesion size, defined as the GFAP-negative area, was observed. D) Subsequently, astrogliosis was determined by measuring GFAP intensity 600 µm caudal and 600 µm cranial from the lesion epicenter. No difference in astrogliosis was observed between the two groups. E) Finally, serotonergic neuron recovery was measured by determining the ratio between the length of 5-HT$^+$ fibers caudal and cranial to the lesion epicenter. The 5-HT$^+$ fiber ratio was significantly increased in ADAM17$^{ex/ex}$ mice compared to ADAM17$^{wt/wt}$ mice. Data are presented as mean ± SEM (B-D = data are expressed as percentage to control). *$p < 0.05$. *ADAM17, 'a disintegrin and metalloproteinase 17'; MBP, myelin basic protein; GFAP, glial fibrillary acidic protein; 5-HT, 5-hydroxytryptamine (serotonin).*

Subsequently, the inflammatory response after SCI was characterized by analyzing the microglia/macrophage infiltration, the presence of pro- and anti-inflammatory macrophages, T helper cells and the number of TMEM119^{+} cells. The microglia/macrophage response was determined by measuring Iba-1 intensity 600 µm caudal and 600 µm cranial from the lesion epicenter. No significant difference in microglia/macrophage response was observed between ADAM17$^{ex/ex}$ and ADAM17$^{wt/wt}$ mice (figure 7A). Next, the presence of M2 macrophages was evaluated by quantifying Arg-1^{+} cells both at the site of injury and perilesional. No difference in the number of Arg-1^{+} cells was observed between the two groups (figure 7B). Investigating the number of infiltrating T helper cells after SCI by quantifying CD4^{+} cells throughout the entire spinal cord revealed a significant increased number of CD4^{+} cells in ADAM17$^{ex/ex}$ mice ($p < 0.01$) compared to ADAM17$^{wt/wt}$ mice (figure 7C). Furthermore, the presence of M1 macrophages was evaluated by quantifying MHC-II^{+} cells at the site of injury and perilesional. The amount of MHC-II^{+} cells was significantly decreased in ADAM17$^{ex/ex}$ mice ($p < 0.05$) compared to ADAM17$^{wt/wt}$ mice (figure 7D-E). Lastly, the number of TMEM119^{+} cells at the site of injury was significantly increased in ADAM17$^{ex/ex}$ mice ($p < 0.01$) compared to ADAM17$^{wt/wt}$ mice (figure 7F-G).

In conclusion, histological analysis of spinal cord tissue revealed an increased demyelinated area and a better recovery of serotonergic fibers in ADAM17$^{ex/ex}$ mice. With regard to the inflammatory response, more TMEM119^{+} microglia as well as CD4^{+} T helper cells and a reduced number of MHC-II^{+} cells were observed in ADAM17$^{ex/ex}$ mice.

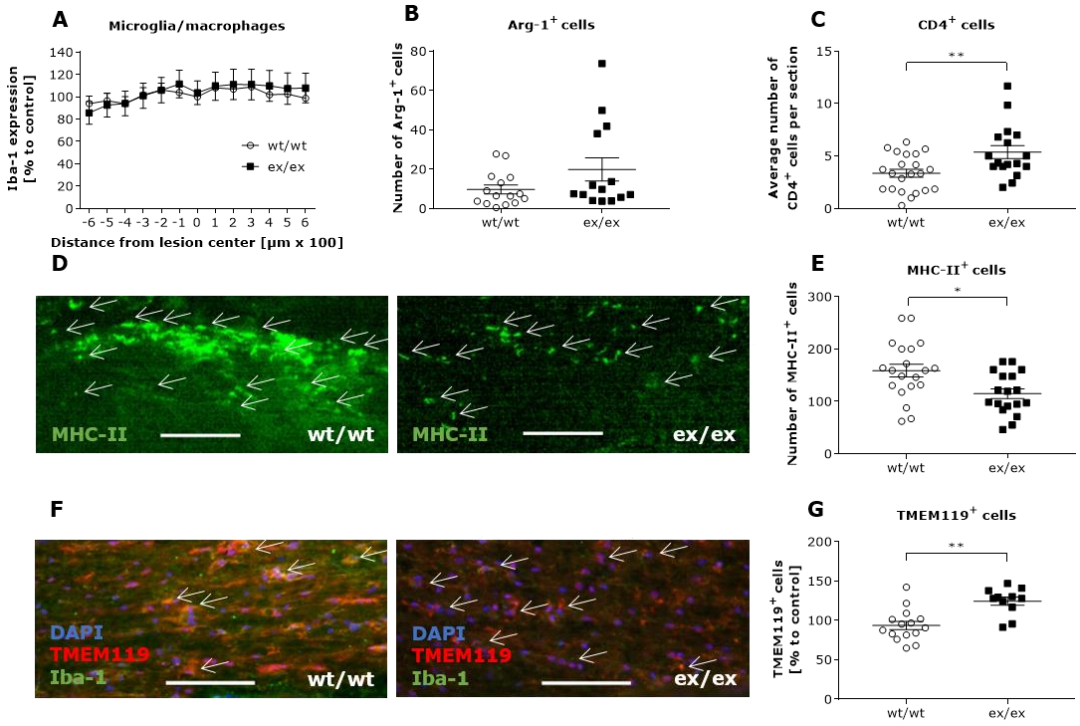

Figure 7: Spinal cord sections from ADAM17$^{ex/ex}$ mice show an increase in CD4$^+$ cells as well as TMEM119$^+$ cells and a decrease in MHC-II$^+$ cells. The inflammatory response after SCI was further characterized in spinal cord tissue of ADAM17$^{ex/ex}$ (ex/ex, n = 9-18) and ADAM17$^{wt/wt}$ mice (wt/wt, n = 13-22). A) First, microglia/macrophage infiltration was analyzed by measuring Iba-1 intensity 600 µm caudal and cranial from the lesion epicenter. No difference in microglia/macrophage infiltration was observed between ADAM17$^{ex/ex}$ and ADAM17$^{wt/wt}$ mice. B) Next, M2 macrophage presence was evaluated by quantifying Arg-1$^+$ cells at the site of injury and perilesional. No difference in the amount of Arg-1$^+$ cells was observed in ADAM17$^{ex/ex}$ mice. C) Furthermore, T helper cell infiltration was investigated by quantifying CD4$^+$ cells throughout the injured spinal cord. CD4$^+$ cell number was significantly increased in ADAM17$^{ex/ex}$ mice compared to ADAM17$^{wt/wt}$ mice. D) Representative images of spinal cord sections from ADAM17$^{wt/wt}$ and ADAM17$^{ex/ex}$ mice stained for MHC-II; arrows indicate MHC-II$^+$ cells. Scale bar: 100 µm. E) The amount of MHC-II$^+$ cells was significantly decreased in ADAM17$^{ex/ex}$ mice compared to ADAM17$^{wt/wt}$ mice. F) Representative images of spinal cord sections from ADAM17$^{wt/wt}$ and ADAM17$^{ex/ex}$ mice stained for TMEM119 and Iba-1; arrows indicate TMEM119$^+$ cells. Scale bar: 100 µm. G) The number of TMEM119$^+$ cells at the site of injury was significantly increased in ADAM17$^{ex/ex}$ mice compared to ADAM17$^{wt/wt}$ mice. Data are presented as mean ± SEM (A, G = data are expressed as percentage to control). *p < 0.05, **p < 0.01. *ADAM17, 'a disintegrin and metalloproteinase 17'; CD4, cluster of differentiation 4; TMEM119, transmembrane protein 119; MHC-II, major histocompatibility complex-II; SCI, spinal cord injury; Iba-1, ionized calcium-binding adapter molecule 1; Arg-1, Arginase-1.*

3.3. ADAM17 deficiency affects gene expression of inflammatory mediators and phagocytic receptors after SCI

In order to determine the effect of ADAM17 deficiency on inflammation and phagocytosis after SCI, spinal cord homogenate was isolated from ADAM17$^{ex/ex}$ and ADAM17$^{wt/wt}$ mice at different time points post-injury. ADAM17 mRNA levels were significantly decreased in ADAM17$^{ex/ex}$ mice at all time points ($p < 0.001$ or $p < 0.0001$) compared to ADAM17$^{wt/wt}$ mice (figure 8A). No difference in the expression of the inflammatory mediator TNF-α was observed between the two groups while IL-1β mRNA expression was significantly increased at 1 ($p < 0.001$) and 7 dpi ($p < 0.01$) in ADAM17$^{ex/ex}$ mice

compared to ADAM17$^{wt/wt}$ mice (figure 8B-C). The expression of the inflammatory cytokine IL-6, the chemokine (C-X-C motif) ligand 1 (CXCL1) and the chemokine (C-C motif) receptor 2 (CCR2) was decreased 3 dpi ($p < 0.01$) in spinal cord homogenate of ADAM17$^{ex/ex}$ mice (figure 8D-F). Furthermore, ADAM17$^{ex/ex}$ mice showed an increased expression of the phagocytic receptor triggering receptor expressed on myeloid cells 2 (TREM2) 3 dpi ($p < 0.01$) and of CD36 ($p < 0.05$) 7 dpi (figure 8G-H). To summarize, ADAM17$^{ex/ex}$ mice showed as expected a reduced expression level of ADAM17. Furthermore, spinal cord homogenate of ADAM17$^{ex/ex}$ mice show a decreased IL-6, CXCL1 and CCR2 expression 3 dpi. On the other hand, IL-1β expression was increased 1 and 7 dpi, TREM2 expression 3 dpi and CD36 expression 7 dpi.

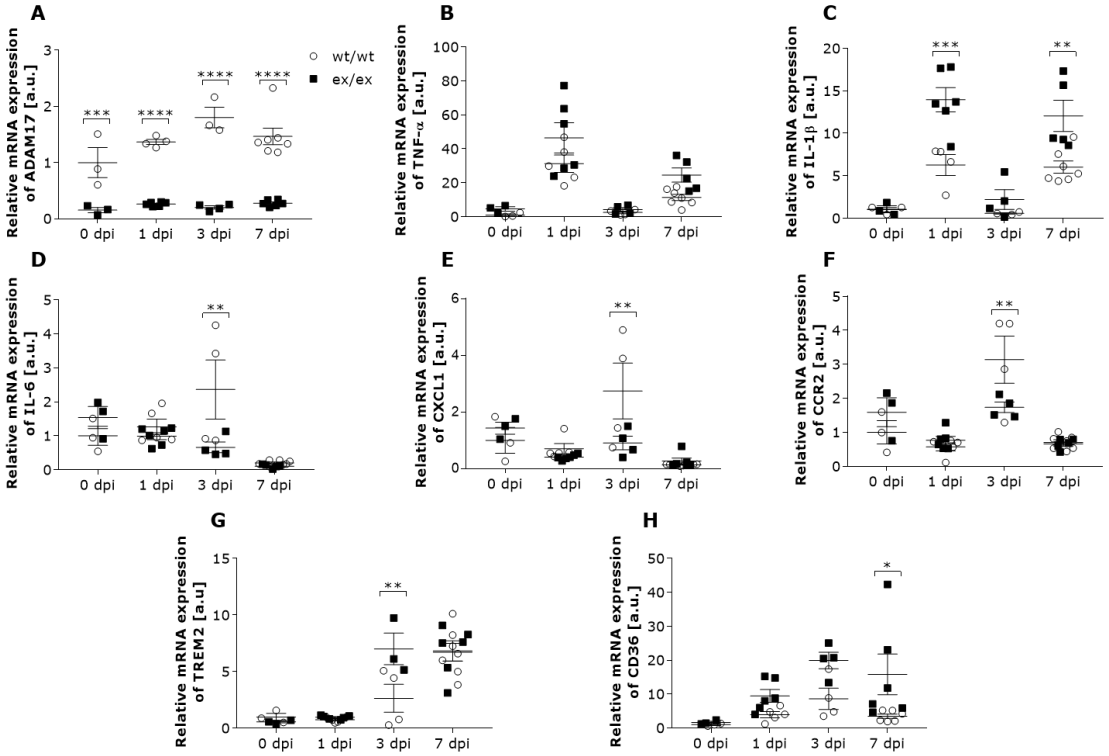

Figure 8: Spinal cord homogenate of ADAM17$^{ex/ex}$ mice show a decreased IL-6, CXCL1 and CCR2 expression but an increased IL-1β expression after SCI. Expression of the phagocytic receptors TREM2 and CD36 was increased 3 or 7 days post-injury, respectively. The gene expression levels of ADAM17, the inflammatory mediators TNF-α, IL-1β, IL-6, CXCL1 and CCR2 and the phagocytic receptors CD36 and TREM2 was determined in spinal cord tissue of ADAM17$^{ex/ex}$ (n = 3-7) and ADAM17$^{wt/wt}$ (n = 3-7) mice by qPCR. A) At all time points, ADAM17 mRNA expression was significantly decreased in ADAM17$^{ex/ex}$ mice compared to ADAM17$^{wt/wt}$ mice. B) TNF-α expression did not differ between the two groups. C) At 1 and 7 dpi, a significant increased IL-1β expression was observed in ADAM17$^{ex/ex}$ mice compared to ADAM17$^{wt/wt}$ mice. D-F) The expression of IL-6, CXCL1 and CCR2 was decreased in ADAM17$^{ex/ex}$ mice at 3 dpi compared to ADAM17$^{wt/wt}$ mice. G-H) ADAM17$^{ex/ex}$ mice showed an increased mRNA expression of TREM2 at 3 dpi and an increased CD36 expression 7 dpi compared to ADAM17$^{wt/wt}$ mice. Relative quantification of gene expression levels was performed by the comparative $2^{-\Delta\Delta CT}$ method. Data were normalized to the most stable reference genes HMBS and GAPDH. Data are presented as mean ± SEM. *$p < 0.05$, **$P < 0.01$, ***$p < 0.001$, ****$p < 0.0001$. *ADAM17, 'a disintegrin and metalloproteinase 17'; IL-6, interleukin-6; CXCL1, chemokine (C-X-C motif) ligand 1; CCR2, chemokine (C-C motif) receptor 2; dpi, days post-injury; TREM2, triggering receptor expressed on myeloid cells 2; CD36, cluster of differentiation 36; TNF-α, tumor necrosis factor-α; qPCR, quantitative polymerase chain reaction; HMBS, hydroxymethylbilane synthase; GAPDH, glyceraldehyde 3-phosphate dehydrogenase.*

3.4. ADAM17 deficiency leads to an increased protein expression of Arg-1 and CD36 after SCI

Next, the effect of ADAM17 deficiency on the anti-inflammatory environment and phagocytosis was evaluated at different time points post-injury. Therefore, the protein expression of the anti-inflammatory M2 macrophage marker Arg-1 and the phagocytic receptor CD36 was determined by western blot analysis in spinal cord homogenate isolated from ADAM17$^{ex/ex}$ and ADAM17$^{wt/wt}$ mice at different time points post-injury. The expression of Arg-1 was significantly increased in ADAM17$^{ex/ex}$ mice 3 dpi ($p < 0.05$) compared to ADAM17$^{wt/wt}$ mice (figure 9A-B). The phagocytic receptor CD36 showed a significantly increased expression in spinal cord homogenate of ADAM17$^{ex/ex}$ mice 28 dpi ($p < 0.05$) (figure 9C-D). In conclusion, ADAM17$^{ex/ex}$ mice showed an increased Arg-1 expression 3 dpi and an increased CD36 expression 28 dpi compared to ADAM17$^{wt/wt}$ mice.

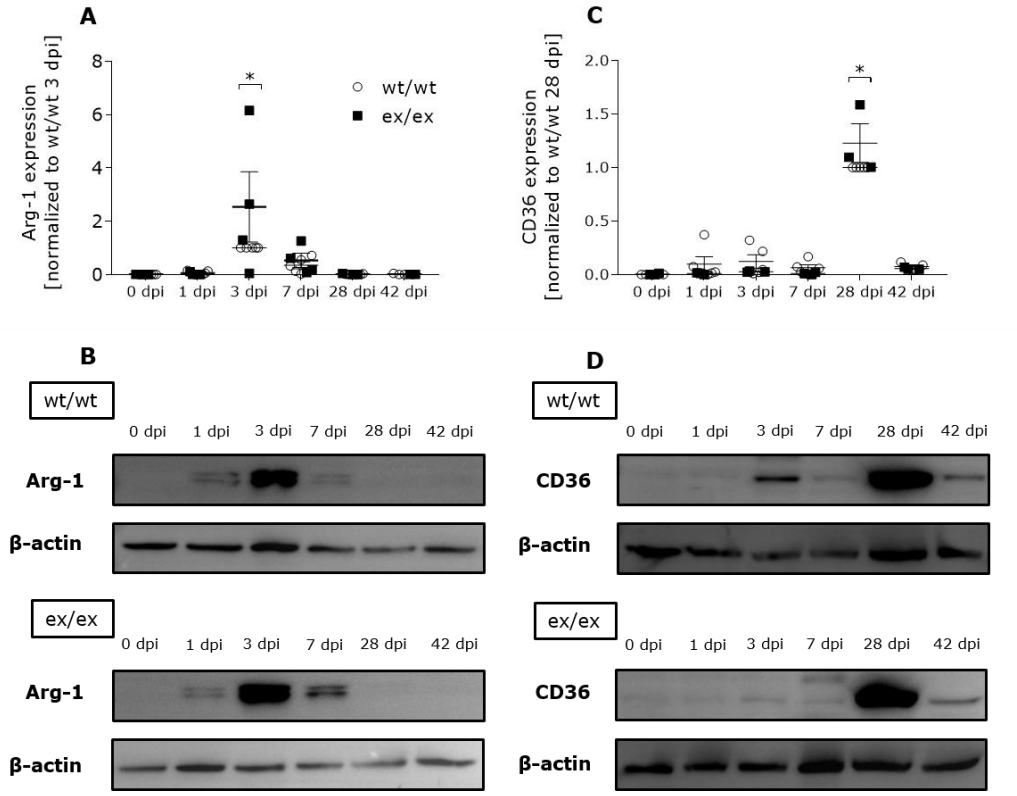

Figure 9: Spinal cord homogenate of ADAM17$^{ex/ex}$ mice shows on protein level an increased expression of Arg-1 and CD36. The protein expression of the M2 macrophage marker Arg-1 and the phagocytic receptor CD36 was determined in spinal cord tissue of ADAM17$^{ex/ex}$ (n = 3-5) and ADAM17$^{wt/wt}$ (n = 4-5) mice by western blot analysis. A) At 3 dpi, Arg-1 expression was significantly increased in ADAM17$^{ex/ex}$ mice compared to ADAM17$^{wt/wt}$ mice (data is normalized to ADAM17$^{wt/wt}$ mice 3 dpi). B) Representative images of western blot analysis performed for Arg-1 (38 kDA). β-actin (42 kDA) is used as a loading control. C) CD36 showed a significantly increased expression in ADAM17$^{ex/ex}$ mice 28 dpi compared to ADAM17$^{wt/wt}$ mice (data is normalized to ADAM17$^{wt/wt}$ mice 28 dpi). D) Representative images of western blot analysis performed for CD36 (53 kDA). β-actin (42 kDA) is used as a loading control. Data are presented as mean ± SEM. *p < 0.05. *ADAM17, 'a disintegrin and metalloproteinase 17'; Arg-1, Arginase-1; CD36, cluster of differentiation 36; dpi, days post-injury.*

3.5. Pharmacological ADAM10/17 inhibition improves functional recovery after SCI

We previously demonstrated that ADAM17 deficiency has a beneficial role in the functional recovery after SCI. Therefore, it was further investigated if the inhibition of ADAM17 by the use of pharmacological inhibitors has a similar effect on the functional recovery after SCI. Mice were treated with an ADAM10/17 inhibitor (GW280264x, GW), a specific ADAM10 inhibitor (GI254023x, GI) or the vehicle (0.6% DMSO in PBS) every day for one week starting 4 hours post-surgery. The functional recovery was evaluated for 28 days using the BMS score (figure 10). The group of mice treated with the ADAM10/17 inhibitor (GW) showed an improvement in functional recovery following SCI ($p < 0.05$) compared to the vehicle treated group. Mice treated with GW also seem to show an improved functional recovery compared to mice treated with the specific ADAM10 inhibitor (GI). However, this difference is not considered statistically significant ($p = 0.0548$). No difference in functional recovery after SCI was observed between the group of mice treated with GI and the vehicle treated group (figure 10). In conclusion, these results indicate that the inhibition of both ADAM10 and ADAM17 improves functional recovery after SCI while the inhibition of ADAM10 alone did not affect functional recovery.

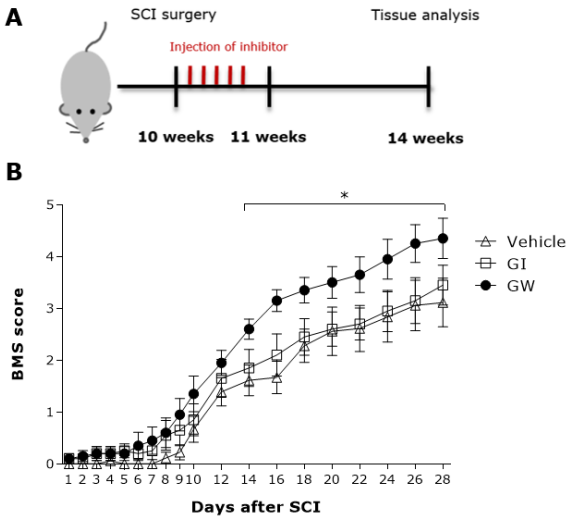

Figure 10: ADAM10/17 inhibition leads to a better functional recovery after SCI. A) 10-week old C57BL/6J mice were subjected to a T-cut hemisection and treated with either an ADAM10/17 inhibitor (GW280264x, GW, n = 10), a specific ADAM10 inhibitor (GI254023x, GI, n = 10) or vehicle (0.6% DMSO in PBS, n = 9) every day for one week starting 4 hours post-surgery. After a 28-day follow-up period, mice were sacrificed and their spinal cord tissue was analyzed. B) The functional recovery of these mice was evaluated for 28 days using the BMS. The GW treated group showed an improved functional recovery after SCI compared to the vehicle treated group. The GW treated mice showed a non-significant improvement in functional recovery compared to the GI treated mice. No difference in functional recovery was observed between the group of mice treated with GI and the vehicle treated mice. Data are presented as mean ± SEM. *$p < 0.05$. *ADAM, 'a disintegrin and metalloproteinase'; SCI, spinal cord injury; DMSO, dimethyl sulfoxide; PBS, phosphate-buffered saline; BMS, Basso Mouse Scale.*

3.6. Inhibition of ADAM10 and ADAM17 reduces the number of MHC-II$^+$ cells

The spinal cord tissue of GW, GI and vehicle treated mice isolated 28 dpi was further analyzed by immunohistochemistry. First, demyelinated area, lesion size and astrogliosis were evaluated by GFAP and MBP staining. GW treated mice showed a trend ($p = 0.0897$) towards a decreased demyelinated area compared to vehicle treated mice (figure 11A-B). No significant differences between the three groups were determined for lesion size (figure 11C). Astrogliosis was analyzed by measuring GFAP intensity beyond the lesion, 600 µm caudal and 600 µm cranial from the lesion epicenter. No significant difference in astrogliosis was observed between the three groups (figure 11D). Furthermore, serotonergic neuron recovery was evaluated by determining the ratio between the length of the 5-HT$^+$ fibers caudal and cranial to the lesion epicenter. This analysis revealed no differences between the three groups (figure 11E).

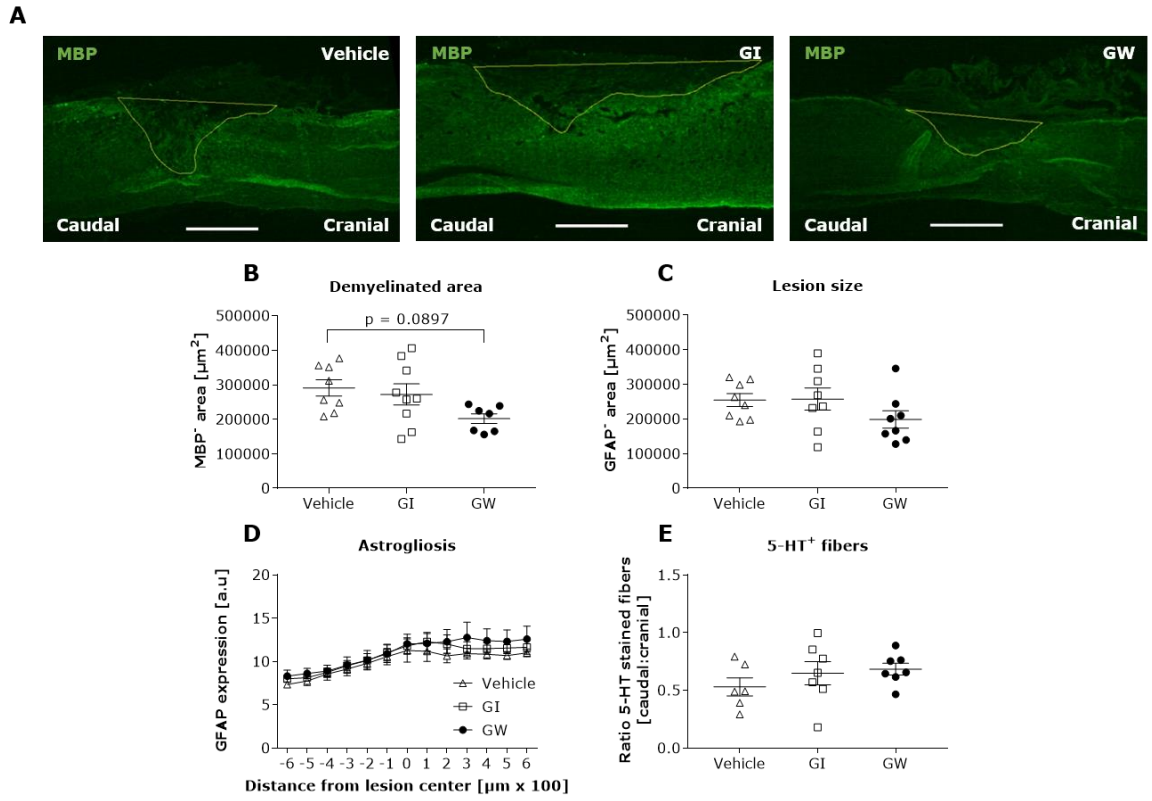

Figure 11: Inhibition of ADAM10 and ADAM17 leads towards a non-significant reduction in the demyelinated area. Spinal cord tissue of mice treated with vehicle (vehicle, n = 6-8), a specific ADAM10 inhibitor GI (GI, n = 7-9) or an ADAM10/17 inhibitor GW (GW, n = 7-8) was further analyzed. A) Representative images of spinal cord sections, including the lesion epicenter, from vehicle, GI or GW treated mice stained for MBP were used to determine the demyelinated area. Scale bar: 500 µm. B) GW treated mice showed a trend towards a reduction of the demyelinated area, the MBP-negative area, compared to the vehicle treated mice. C) Lesion size, defined as the GFAP-negative area, showed no differences between the three groups. D) Subsequently, astrogliosis was evaluated by measuring GFAP intensity 600 µm caudal and 600 µm cranial from the lesion epicenter. No significant difference in astrogliosis was observed between the three groups. E) Furthermore, serotonergic neuron recovery was evaluated by determining the ratio between the length of the 5-HT$^+$ fibers caudal and cranial to the lesion epicenter. This analysis revealed no differences between the three groups. Data are presented as mean ± SEM. *ADAM, 'a disintegrin and metalloproteinase'; MBP, myelin basic protein; GFAP, glial fibrillary acidic protein; 5-HT, 5-hydroxytryptamine (serotonin).*

Next, the immune response after SCI was characterized by determining the presence of pro- and anti-inflammatory macrophages, T helper cells and microglia/macrophage infiltration. The pro-inflammatory M1 macrophages and anti-inflammatory M2 macrophages, MHC-II$^+$ and Arg-1$^+$ cells respectively, were quantified at the site of injury and perilesional. A significantly decreased number of MHC-II$^+$ cells was observed in the GI and the GW treated mice ($p < 0.05$) compared to the vehicle treated group (figure 12A-B), while no difference in the number of Arg-1$^+$ cells was determined (figure 12C). Furthermore, no difference in microglia/macrophage infiltration (Iba-1 staining) was observed between the three groups (figure 12D). Finally, the presence of T helper cells was determined by counting the number of CD4$^+$ cells throughout the entire spinal cord. The number of CD4$^+$ cells did not significantly differ between the three groups (figure 12E). In conclusion, GW treatment leads towards a non-significant reduction in the demyelinated area. GI and GW treated mice showed a decreased number of MHC-II$^+$ cells while no differences were revealed in lesion size, astrogliosis, 5-HT$^+$ fiber ratio, microglia/macrophage infiltration, Arg-1$^+$ cells or CD4$^+$ cells.

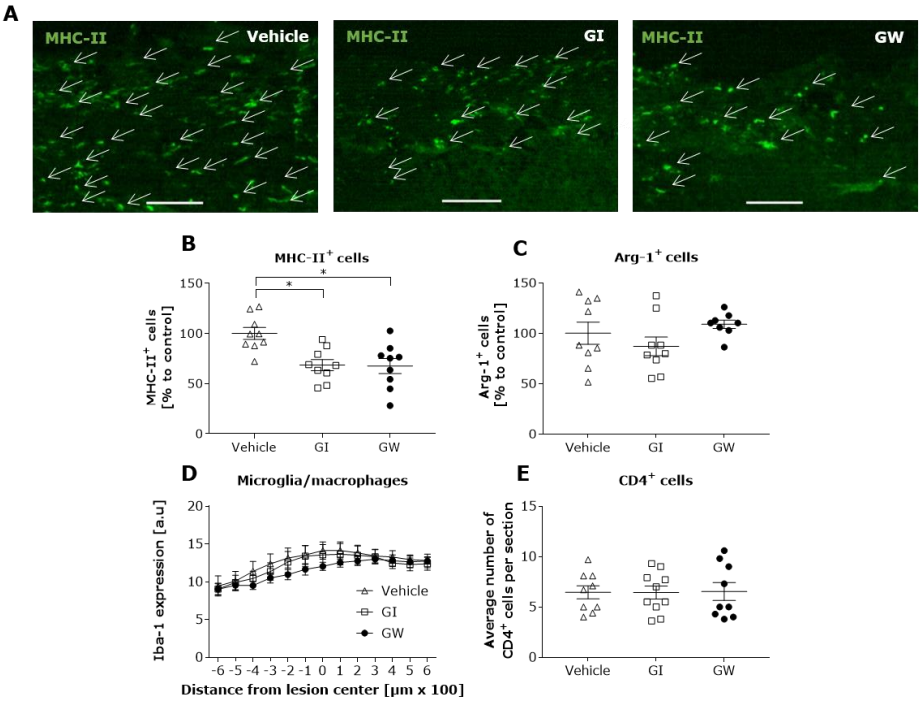

Figure 12: Inhibition of ADAM10 and ADAM10/17 reduces the number of MHC-II$^+$ cells. Spinal cord tissue of mice treated with the vehicle (vehicle, n = 8-9), the specific ADAM10 inhibitor GI (GI, n = 8-10) or the ADAM10/17 inhibitor GW (GW, n = 7-10) was further analyzed. A) Representative images of spinal cord sections from vehicle, GI or GW treated mice stained for MHC-II; white arrows indicate MHC-II$^+$ cells. Scale bar: 100 µm. B-C) The presence of M1 and M2 macrophages, MHC-II$^+$ and Arg-1$^+$ cells respectively, was quantified at the site of injury and perilesional. A decreased number of MHC-II$^+$ cells was observed in GI or GW treated mice compared to the vehicle treated mice, while no difference was observed in the number of Arg-1$^+$ cells. D) Iba-1 staining was used to determine microglia/macrophage infiltration 600 µm caudal and cranial from the lesion epicenter. No difference in microglia/macrophage response was observed between the three groups. E) The presence of T helper cells was determined by quantifying CD4$^+$ cell number throughout the entire spinal cord. The amount of CD4$^+$ cells did not differ between the three groups. Data are presented as mean ± SEM (B-C = data are expressed as percentage to control). *$p < 0.05$. *ADAM, 'a disintegrin and metalloproteinase'; MHC-II, major histocompatibility complex-II; Arg-1, Arginase-1; Iba-1, ionized calcium-binding adapter molecule 1; CD4, cluster of differentiation 4.*

3.7. Microglia-specific ADAM17 knockout mice show a better functional recovery after SCI

Based on our previous results indicating that ADAM17 deficiency or the inhibition of ADAM17 leads to a better functional recovery after SCI (figure 5, 10), the main cell type responsible for this effect was further investigated. Due to their localization in the CNS and their immediate response after injury, microglia are one of the main actors during SCI inflammation. Therefore, a mouse model with a tamoxifen-inducible microglia-specific ADAM17 knockout (ADAM17flox$^{+/+}$-Cx3Cr1-CreERT2) was generated. In this mouse model, Cre-recombination is driven under the Cx3Cr1 promotor. This promotor is expressed in monocytes, monocyte-derived macrophages, tissue-specific macrophages and microglia (42, 43). Therefore, ADAM17flox$^{+/+}$-Cx3Cr1-Cre$^{+/-}$ mice have upon tamoxifen treatment not only an ADAM17 knockout in microglia but also in monocytes and macrophages. However, the ADAM17 knockout in monocytes and macrophages disappears due to their repopulation while ADAM17 knockout persists in microglia 6 weeks post-tamoxifen treatment (43). The efficiency of Cre-lox recombination and the subsequent ADAM17 knockout in microglia was confirmed by qPCR and western blot (figure S1). In this way, the effect of microglial ADAM17 knockout on the functional recovery after SCI was studied. Siblings lacking Cre-recombinase (ADAM17flox$^{+/+}$-Cx3Cr1-Cre$^{-/-}$) were also treated with tamoxifen and used as a control group. ADAM17flox$^{+/+}$-Cx3Cr1-Cre$^{+/-}$ and ADAM17flox$^{+/+}$-Cx3Cr1-Cre$^{-/-}$ mice were subjected to a T-cut hemisection and the functional recovery was assessed for 28 days using the BMS. From day 8 onwards, locomotor function of ADAM17flox$^{+/+}$-Cx3Cr1-Cre$^{+/-}$ mice was significantly improved ($p < 0.01$) compared to ADAM17flox$^{+/+}$-Cx3Cr1-Cre$^{-/-}$ mice (figure 13). In conclusion, these results show that microglia-specific ADAM17 knockout improves functional recovery after SCI.

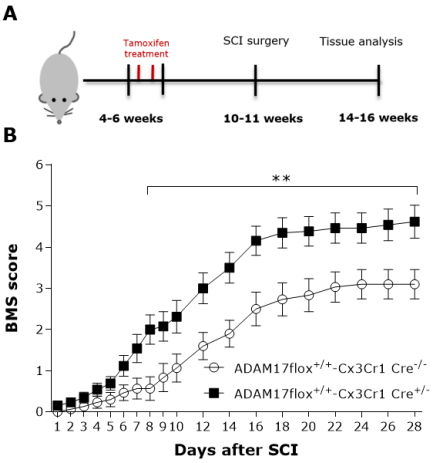

Figure 13: Microglia-specific ADAM17 knockout mice have a better functional recovery after SCI. A) At the age of 4 to 6 weeks, ADAM17flox$^{+/+}$-Cx3Cr1-Cre$^{+/-}$ (n = 13) and ADAM17flox$^{+/+}$-Cx3Cr1-Cre$^{-/-}$ mice (n = 15) were treated twice every other day with tamoxifen to induce a microglia-specific ADAM17 knockout in ADAM17flox$^{+/+}$-Cx3Cr1-Cre$^{+/-}$ mice. At the age of 10 to 12 weeks, these mice were subjected to a T-cut hemisection. After a 28-day follow-up period, mice were sacrificed and their spinal cord tissue was analyzed. B) The functional recovery of these mice was evaluated for 28 days using the BMS. ADAM17flox$^{+/+}$-Cx3Cr1-Cre$^{+/-}$ mice showed an improved functional recovery after SCI compared to ADAM17flox$^{+/+}$-Cx3Cr1-Cre$^{-/-}$ mice. Data are presented as mean ± SEM. **p < 0.01. *ADAM17, 'a disintegrin and metalloproteinase 17'; SCI, spinal cord injury; BMS, Basso Mouse Scale.*

3.8. Microglia-specific ADAM17 knockout affects serotonergic neuron recovery and the inflammatory response after SCI

Spinal cord tissue of ADAM17flox$^{+/+}$-Cx3Cr1-Cre$^{+/-}$ and ADAM17flox$^{+/+}$-Cx3Cr1-Cre$^{-/-}$ mice was further analyzed by immunohistochemistry 28 dpi. First, demyelinated area, lesion size and astrogliosis was determined by MBP and GFAP immunofluorescence. No significant differences in lesion size and demyelinated area were observed between the two groups (figure 14A-B). Astrogliosis after SCI was determined by measuring GFAP intensity 600 µm caudal and 600 µm cranial from the lesion epicenter. No significant difference in astrogliosis was observed between ADAM17flox$^{+/+}$-Cx3Cr1-Cre$^{+/-}$ and ADAM17flox$^{+/+}$-Cx3Cr1-Cre$^{-/-}$ mice 28 dpi (figure 14C). Next, serotonergic neuron recovery was evaluated by determining the ratio between the length of 5-HT^{+} fibers caudal and cranial to the lesion epicenter. A trend (p = 0.065) towards an increased ratio was observed in ADAM17flox$^{+/+}$-Cx3Cr1-Cre$^{+/-}$ mice compared to ADAM17flox$^{+/+}$-Cx3Cr1-Cre$^{-/-}$ mice (figure 14D).

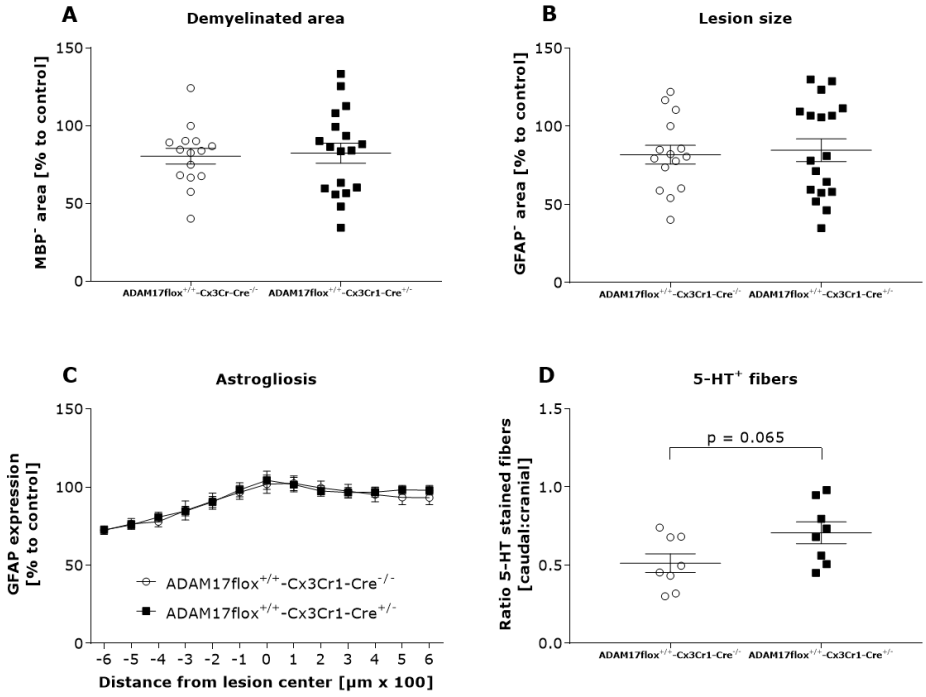

Figure 14: Microglia-specific ADAM17 knockout mice show a suggestive trend towards an increased 5-HT^{+} fiber ratio. Spinal cord tissue of ADAM17flox$^{+/+}$-Cx3Cr1-Cre$^{+/-}$ (n = 8-18) and ADAM17flox$^{+/+}$-Cx3Cr1-Cre$^{-/-}$ mice (n = 8-18) was further analyzed. A-B) Demyelinated area and lesion size, respectively defined as the MBP and GFAP-negative area, showed no differences between ADAM17flox$^{+/+}$-Cx3Cr1-Cre$^{+/-}$ and ADAM17flox$^{+/+}$-Cx3Cr1-Cre$^{-/-}$ mice. C) Astrogliosis, determined by measuring GFAP intensity 600 µm caudal and 600 µm cranial from the lesion epicenter, showed no differences between the two groups. D) Serotonergic neuron recovery was evaluated by determining the ratio between the length of the 5-HT^{+} fibers caudal and cranial to the lesion epicenter. ADAM17flox$^{+/+}$-Cx3Cr1-Cre$^{+/-}$ mice showed a trend towards an increased ratio compared to ADAM17flox$^{+/+}$-Cx3Cr1-Cre$^{-/-}$ mice. Data are presented as mean ± SEM (A-C = data are expressed as percentage to control). *ADAM17, 'a disintegrin and metalloproteinase 17'; 5-HT, 5-hydroxytryptamine (serotonin); GFAP, glial fibrillary acidic protein; MBP, myelin basic protein.*

Subsequently, the inflammatory response after SCI was characterized by analyzing microglia/macrophages infiltration and the presence of T helper cells, M1 and M2 macrophages. The microglia/macrophage response was determined by measuring Iba-1 intensity 600 µm caudal and 600 µm cranial from the lesion epicenter. ADAM17flox$^{+/+}$-Cx3Cr1-Cre$^{+/-}$ mice showed a decreased microglia/macrophage infiltration at 28 dpi ($p < 0.05$) compared to ADAM17flox$^{+/+}$-Cx3Cr1-Cre$^{-/-}$ mice (figure 15A-B). The infiltration of T helper cells was investigated by counting the CD4$^+$ cells throughout the spinal cord. However, the amount of CD4$^+$ cells was comparable between the two groups (figure 15C).

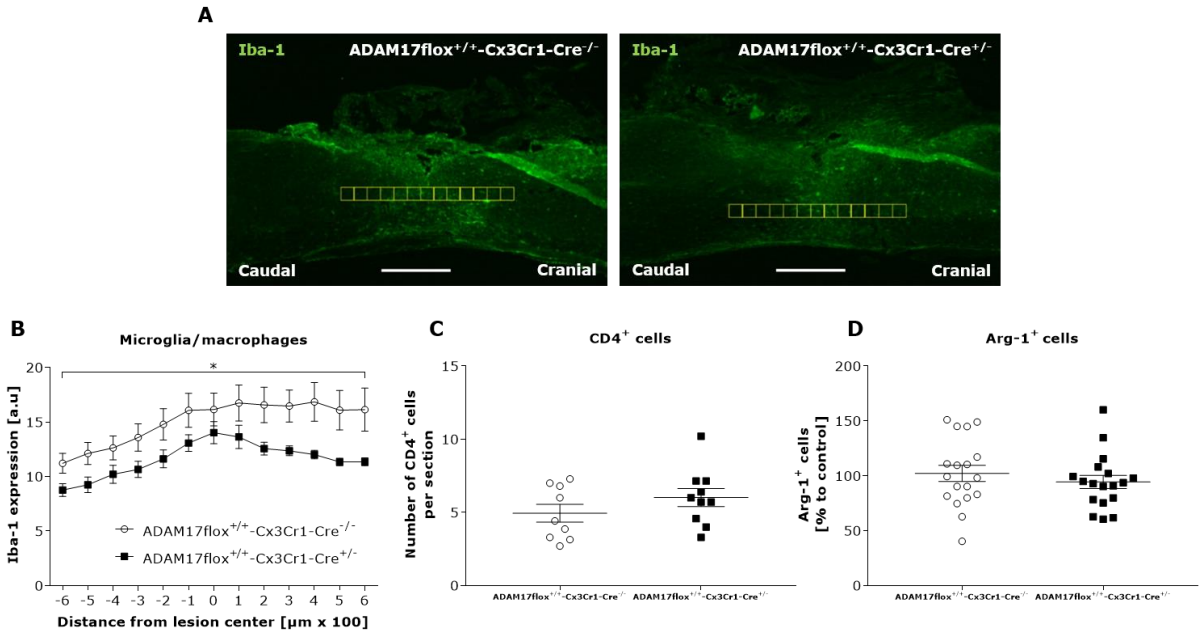

Figure 15: Microglia-specific ADAM17 knockout mice show a decreased microglia/macrophage infiltration. Spinal cord tissue of ADAM17flox$^{+/+}$-Cx3Cr1-Cre$^{+/-}$ (n = 7-18) and ADAM17flox$^{+/+}$-Cx3Cr1-Cre$^{-/-}$ mice (n = 10-18) was further analyzed. A) Representative images of spinal cord sections, including the lesion epicenter, from ADAM17flox$^{+/+}$-Cx3Cr1-Cre$^{+/-}$ and ADAM17flox$^{+/+}$-Cx3Cr1-Cre$^{-/-}$ mice stained for Iba-1 were used to determine microglia/macrophage infiltration. Scale bar: 500 µm. B) Microglia/macrophage infiltration was determined by measuring Iba-1 intensity 600 µm caudal and 600 µm cranial of the lesion epicenter. A significant decrease in the microglia/macrophage response was observed in ADAM17flox$^{+/+}$-Cx3Cr1-Cre$^{+/-}$ mice compared to ADAM17flox$^{+/+}$-Cx3Cr1-Cre$^{-/-}$ mice. C) Infiltration of T helper cells after SCI was investigated by quantifying the CD4$^+$ cells throughout the spinal cord. The amount of CD4$^+$ cells was comparable between ADAM17flox$^{+/+}$-Cx3Cr1-Cre$^{+/-}$ and ADAM17flox$^{+/+}$-Cx3Cr1-Cre$^{-/-}$ mice at 28 dpi. D) Next, the presence of M2 macrophages was evaluated by quantifying Arg-1$^+$ cells at the site of injury and perilesional. No difference in the amount of Arg-1$^+$ cells was observed between the two groups. Data are presented as mean ± SEM (D = data are expressed as percentage to control). *$p < 0.05$. *ADAM17, 'a disintegrin and metalloproteinase 17'; Iba-1, ionized calcium-binding adapter molecule 1; CD4, cluster of differentiation; dpi, days post-injury; Arg-1, Arginase-1.*

Next, the presence of anti-inflammatory M2 macrophages and pro-inflammatory M1 macrophages was evaluated by quantifying the Arg-1$^+$ and MHC-II$^+$ cells at the site of injury and perilesional. No difference in the amount of Arg-1$^+$ cells was observed between the two groups (figure 15D), while the number of MHC-II$^+$ cells was significantly decreased in ADAM17flox$^{+/+}$-Cx3Cr1-Cre$^{+/-}$ mice ($p < 0.01$) compared to ADAM17flox$^{+/+}$-Cx3Cr1-Cre$^{-/-}$ mice (figure 16A-B).

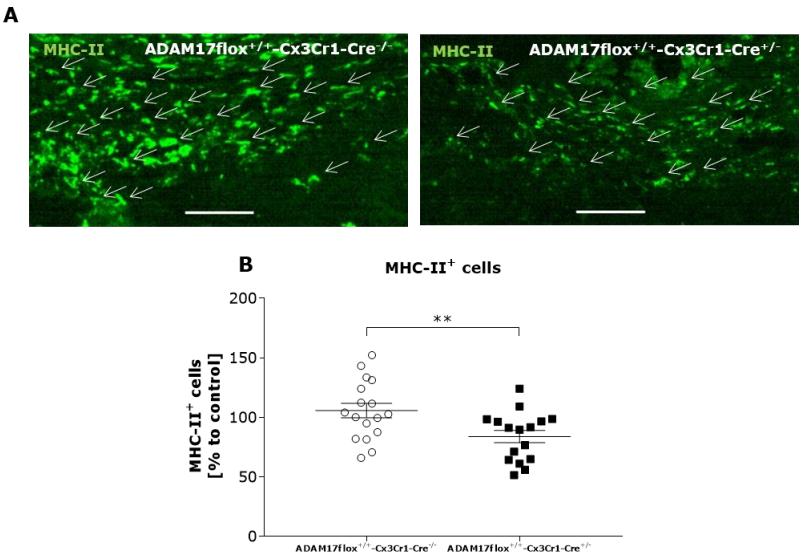

Figure 16: Microglia-specific ADAM17 knockout mice show a decreased number of MHC-II$^+$ cells. Spinal cord tissue of ADAM17flox$^{+/+}$-Cx3Cr1-Cre$^{+/-}$ (n =16) and ADAM17flox$^{+/+}$-Cx3Cr1-Cre$^{-/-}$ mice (n = 17) was further analyzed. A) Representative images of spinal cord sections from ADAM17flox$^{+/+}$-Cx3Cr1-Cre$^{+/-}$ and ADAM17flox$^{+/+}$-Cx3Cr1-Cre$^{-/-}$ mice stained for MHC-II; arrows indicate MHC-II$^+$ cells. Scale bar: 100 µm. B) The amount of MHC-II$^+$ cells was significantly decreased in ADAM17flox$^{+/+}$-Cx3Cr1-Cre$^{+/-}$ mice compared to ADAM17flox$^{+/+}$-Cx3Cr1-Cre$^{-/-}$ mice. Data are presented as mean ± SEM (B = data are expressed as percentage to control). **p < 0.01. *ADAM17, 'a disintegrin and metalloproteinase 17'; MHC-II, major histocompatibility complex-II.*

To summarize, microglia-specific ADAM17 knockout mice showed a significantly decreased microglia/macrophage infiltration, number of MHC-II$^+$ cells and a trend towards an increased 5-HT$^+$ fiber ratio. Microglia-specific ADAM17 knockout does not affect lesion size, demyelinated area, astrogliosis and the presence of Arg-1$^+$ and CD4$^+$ cells.

3.9. ADAM17 affects differentially the phagocytic capacity of BMDMs and primary microglia

After SCI, phagocytosis of cellular debris by monocyte-derived macrophages and microglia plays an important role in diminishing inflammation and in initiating repair processes. Since ADAM17 is involved in the shedding of several phagocytic receptors, such as CD36 and MerTK, we further investigated the effect of ADAM17 deficiency on the phagocytic capacity of BMDMs and primary microglia. BMDMs and microglia isolated from ADAM17$^{ex/ex}$ or ADAM17$^{wt/wt}$ mice were first overnight stimulated with an M1 (LPS or IFN-γ) or an M2 stimulus (IL-4). These cells were exposed to latex beads or apoptotic Neuro-2a cells for 1.5 hours. Thereafter, the percentage of BMDMs or microglia that engulfed latex beads or apoptotic cells was quantified by FACS analysis. Untreated and IFN-γ stimulated ADAM17$^{ex/ex}$ BMDMs showed a significantly decreased phagocytic capacity of latex beads ($p < 0.01$ and $p < 0.0001$, respectively) compared to ADAM17$^{wt/wt}$ BMDMs, while no difference in phagocytic capacity was observed for LPS or IL-4 stimulated ADAM17$^{ex/ex}$ BMDMs (figure 17A). On the other hand, untreated and IL-4 treated ADAM17$^{ex/ex}$ BMDMs showed an increased phagocytic capacity ($p < 0.05$) of apoptotic Neuro-2a cells compared to ADAM17$^{wt/wt}$ BMDMs. However, no

difference in phagocytic capacity was observed in LPS or IFN-γ treated ADAM17$^{ex/ex}$ BMDMs (figure 17B). Furthermore, an increased phagocytosis of latex beads was observed in LPS stimulated ADAM17$^{ex/ex}$ microglia compared to ADAM17$^{wt/wt}$ microglia ($p < 0.0001$). No differences in phagocytosis were shown in untreated, IFN-γ or IL-4 stimulated microglia (figure 17C). In conclusion, untreated or IFN-γ stimulated ADAM17$^{ex/ex}$ BMDMs showed a decreased phagocytosis of latex beads, while an increased phagocytic capacity of apoptotic Neuro-2a cells was observed in untreated or IL-4 stimulated ADAM17$^{ex/ex}$ BMDMs. Whereas an increased phagocytic capacity of latex beads was observed in LPS stimulated ADAM17$^{ex/ex}$ microglia.

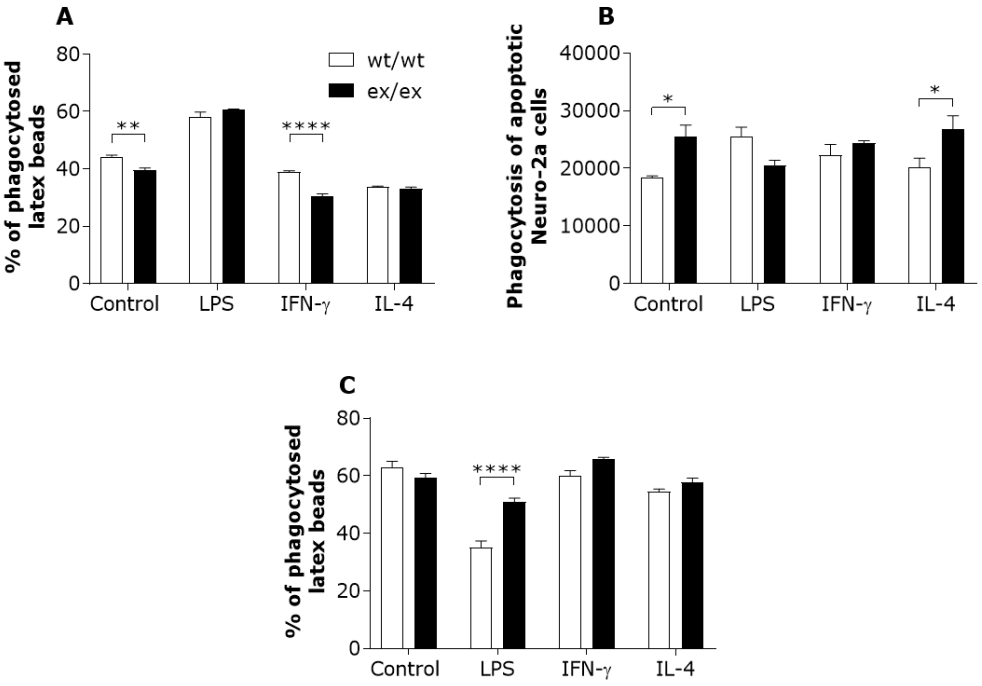

Figure 17: Differences in the phagocytic capacity of BMDMs and primary microglia isolated from ADAM17$^{ex/ex}$ mice. BMDMs and primary microglia isolated from ADAM17$^{ex/ex}$ and ADAM17$^{wt/wt}$ mice were first overnight stimulated with an M1 stimuli (LPS or IFN-γ) or M2 stimulus (IL-4). These cells were exposed to latex beads or apoptotic Neuro-2a cells for 1.5 hours. Thereafter, the phagocytic capacity of BMDMs and microglia was quantified by FACS analysis. A) Untreated and IFN-γ stimulated ADAM17$^{ex/ex}$ BMDMs phagocytosed significantly less latex beads compared to ADAM17$^{wt/wt}$ BMDMs. B) Furthermore, untreated and IL-4 treated ADAM17$^{ex/ex}$ BMDMs phagocytosed significantly more apoptotic Neuro-2a cells compared to ADAM17$^{wt/wt}$ BMDMs. C) Primary microglia of ADAM17$^{ex/ex}$ mice show a higher phagocytic capacity of latex beads upon LPS stimulation compared to ADAM17$^{wt/wt}$ microglia. A-C = Representative graphs of the different experiments are shown. Data are presented as mean ± SEM. *$p < 0.05$, **$P < 0.01$, ****$p < 0.0001$. *BMDMs, bone marrow-derived macrophages; ADAM17, 'a disintegrin and metalloproteinase 17'; LPS, lipopolysaccharide; IFN-γ, interferon-gamma; IL-4, interleukin-4; FACS, fluorescence-activated cell sorting.*

4. Discussion

After SCI, an excessive inflammatory response is provoked which is considered the major contributor to secondary damage (8). Despite the dual character of inflammation after SCI, the injured spinal cord favors a strong pro-inflammatory reaction that aggravates the primary injury by damaging healthy tissue. Therefore, a shift towards a more anti-inflammatory response, necessary for the clearance of cellular debris preventing neuron regeneration, is considered a potential therapeutic strategy after SCI (7, 8, 13, 14). After SCI, phagocytosis of cellular debris by professional phagocytes such as resident microglia and monocyte-derived macrophages is an important mechanism to diminish inflammation and to initiate repair processes (14, 34). The involvement of the enzyme ADAM17 in shedding various inflammatory mediators (such as the pro-inflammatory cytokine TNF-α and the cytokine receptors TNF-R and IL-6R) and phagocytic receptors (including CD36 and MerTK) makes this enzyme an interesting target to modulate inflammation and the phagocytic activity of for instance resident microglia and monocyte-derived macrophages (24, 26). In this study, we therefore hypothesized that ADAM17 deficiency favors an anti-inflammatory environment by reducing the shedding of inflammatory mediators and by enhancing the resolution of inflammation through phagocytosis leading to an improved functional recovery after SCI.

First, the effect of ADAM17 deficiency and its pharmacological inhibition was investigated in an *in vivo* mouse model of SCI. Therefore, either ADAM17$^{ex/ex}$ mice were used with an almost complete absence of functional ADAM17 protein in the whole organism or ADAM17 was systemically inhibited by an ADAM10/17 inhibitor (24). A well-established model of a T-cut hemisection was used to generate a standardized lesion without spared fibers (38, 44). ADAM17 deficiency as well as its pharmacological inhibition lead to a significantly improved functional recovery after SCI.

Surprisingly, on histological level ADAM17 deficiency or its pharmacological inhibition did affect neither lesion size nor astrogliosis. However, a significant increased demyelinated area was determined in spinal cord tissue of ADAM17$^{ex/ex}$ mice. Postnatal CNS myelination is disturbed in ADAM17$^{ex/ex}$ mice since Palazuelos *et al.* identified ADAM17 as a key modulator of oligodendrocyte development, so-called oligodendrogenesis. ADAM17 regulates oligodendrogenesis via the shedding of the EGFR ligand TGF-α and heparin binding EGF-like growth factor and the subsequent activation of EGFR signaling in oligodendrocyte lineage cells necessary for their survival and oligodendrocyte precursor proliferation (45). Besides, ADAM17 is also involved in modulating oligodendrogenesis in the context of oligodendrocyte regeneration and CNS remyelination. Therefore, the deficiency of ADAM17 after SCI blunts oligodendrocyte precursor expansion and oligodendrocyte regeneration causing a delay in CNS remyelination (46). Furthermore, ADAM17 deficiency leads to an increase in the ratio between the length of 5-HT^{+} fibers caudal and cranial to the lesion epicenter, which is suggestive for the recovery of serotonergic neurons 4 weeks post-injury. The involvement of 5-HT in modulating motor function by regulating the rhythm and coordination of movements indicates that serotonergic neuron recovery is related to an improved functional recovery after SCI, as observed in hypomorphic ADAM17 mice (47).

The inflammatory reaction after SCI was subsequently characterized in ADAM17$^{ex/ex}$ mice and mice treated with the ADAM10/17 inhibitor. Microglia were quantified using TMEM119 immunostaining,

which Bennett *et al.* identified as a microglia-specific cell surface marker not expressed by macrophages, other immune cells or neural cell types (48). Evaluation of microglia in ADAM17$^{ex/ex}$ mice observed an increased number of TMEM119^{+} cells at the site of injury. On the one hand, microglia can aggravate the inflammatory response by the release of pro-inflammatory mediators (14, 16). On the other hand, microglia can also exert a beneficial role during inflammation by the release of neurotrophic factors (including insulin-like growth factor-1 or brain derived neurotrophic factor), phagocytosis of cellular debris leading to a reduced inflammation and initiation of repair or the formation of a border around the lesion that blocks the spread of damage (14, 16, 17, 49). Since TMEM119 does not distinguish these phenotypes, no conclusion is taken regarding the inflammatory character of these microglia. However, the improved functional recovery observed after SCI in ADAM17$^{ex/ex}$ mice may suggest that microglia with a beneficial role are predominant in these mice.

In spinal cord sections of ADAM17$^{ex/ex}$ mice and mice treated with the ADAM10/17 inhibitor, a reduced number of MHC-II^{+} cells, representing the pro-inflammatory M1 microglia/macrophages, was determined at the lesion site and perilesional 28 dpi compared to the respective control groups. As M1 macrophages release and produce pro-inflammatory and cytotoxic mediators, a decrease in this phenotype contributes to a reduction in the pro-inflammatory environment of the spinal cord (8, 14, 20). The reduced inflammatory environment in these mice corresponds to the observed improvement in their functional recovery. T cell analysis within the spinal cord showed a significantly increased number of CD4^{+} T cells in ADAM17$^{ex/ex}$ mice. However, the specific T cell subtype is unclear, since T cell phenotyping after CNS injury is challenging due to the low number of T cells present in the CNS (50).

The expression of the anti-inflammatory M2 macrophage marker Arg-1 was further investigated at different time points post-injury in spinal cord homogenate of ADAM17$^{ex/ex}$ and ADAM17$^{wt/wt}$ mice. Our results reveal that Arg-1 is only expressed during the first week following SCI while its expression disappears 28 or 42 dpi. As already shown in a study by Kigerl *et al.*, analysis of the expression of various M1 and M2 macrophage markers demonstrates that the anti-inflammatory M2 macrophage response is initiated rapidly after SCI but dissipated after the first week following SCI (20). This study also explains the low number of Arg-1^{+} cells observed 28 dpi by immunohistochemistry. Furthermore, our results reveal a significantly increased expression of Arg-1 3 dpi in ADAM17$^{ex/ex}$ mice, which indicates an increased anti-inflammatory environment in their spinal cord during the first week following SCI. This modification to the micro-environment of the spinal cord in ADAM17$^{ex/ex}$ mice correlates to their improved functional recovery after SCI.

Further analysis of the inflammatory response in the spinal cord reveals a significantly decreased IL-6, CXCL1 and CCR2 mRNA expression in ADAM17$^{ex/ex}$ mice while IL-1β mRNA expression is significantly increased in the acute and subacute phase after SCI. These results indicate a change in the inflammatory environment of the spinal cord. On the one hand, the increased expression of IL-1β is shown to be detrimental after SCI (51) while a decreased IL-6, CXCL1 and CCR2 expression is proven to be beneficial after SCI (52-54). Until now, we only determined gene expression of cytokines and chemokines in the spinal cord, while the protein expression of these inflammatory mediators should be further investigated. Surprisingly, our results show no change in TNF-α mRNA expression in spinal cords of ADAM17$^{ex/ex}$ mice compared to ADAM17$^{wt/wt}$ mice while an increased

expression of membrane-bound TNF-α was expected due to an impaired shedding of TNF-α in ADAM17$^{ex/ex}$ mice. This finding is supported by other studies which suggest that the expression of membrane-bound TNF-α may be regulated by a feedback mechanism independent of shedding by ADAM17 (35, 55). However, further research to confirm this finding is necessary by measuring TNF-α expression on the protein level since TNF-α expression is regulated both transcriptionally and post-transcriptionally. Post-transcriptional regulation of TNF-α expression is affected by AU-rich elements expression in the 3'-untranslated region of transcripts encoding cytokines, oncoproteins, growth and transcription factors. These elements play an important role in controlling TNF-α mRNA stability and translation which contributes to the promotion or the inhibition of TNF-α expression (56). Furthermore, it would be useful to determine cytokine and chemokine levels in the serum of ADAM17$^{ex/ex}$ and ADAM17$^{wt/wt}$ mice which would provide more information on the effect of ADAM17 deficiency on the systemic inflammatory reaction after SCI.

Based on our previous findings, the main cell type responsible for the beneficial effect of ADAM17 deficiency or its pharmacological inhibition after SCI was further determined. Resident microglia are one of the main actors during SCI inflammation because of their localization in the CNS and their immediate response after SCI (14, 16). Therefore, a T-cut hemisection was induced in a mouse model with a tamoxifen-inducible microglia-specific ADAM17 knockout (ADAM17flox$^{+/+}$-Cx3Cr1-Cre$^{+/-}$) to study the effect of microglial ADAM17 on the functional recovery after SCI. ADAM17flox$^{+/+}$-Cx3Cr1-Cre$^{+/-}$ mice showed an improved functional recovery after SCI indicating that microglial ADAM17 is playing an important role in the beneficial effect of ADAM17 deficiency or inhibition on functional recovery after SCI. As observed on the histological level in spinal cord sections of hypomorphic ADAM17 mice, we also observed a suggestive trend towards a higher ratio between the length of the 5-HT^{+} fibers caudal and cranial to the lesion epicenter in ADAM17flox$^{+/+}$-Cx3Cr1-Cre$^{+/-}$ mice. As described above, this might be related to the improved functional recovery.

Characterization of the inflammatory response after SCI showed a decrease in the number of MHC-II^{+} cells and microglia/macrophages infiltration in ADAM17flox$^{+/+}$-Cx3Cr1-Cre$^{+/-}$ mice. The decrease in MHC-II^{+} cells corresponds to our findings in ADAM17$^{ex/ex}$ mice and mice treated with the ADAM10/17 inhibitor. Besides, ADAM17flox$^{+/+}$-Cx3Cr1-Cre$^{+/-}$ mice also showed a reduction in the microglia/macrophages infiltration into the spinal cord. The reduced microglia/macrophages infiltration is at least partially explained by the reduced number of MHC-II^{+} cells. Since Iba-1 does not distinguish microglia and macrophages, microglia-specific TMEM119 staining would provide more information about the number of microglia present at the lesion epicenter (48). As described above, a reduction in M1 macrophages which release and produce pro-inflammatory and cytotoxic mediators contributes to a less pro-inflammatory environment (8, 14, 20). This change in the inflammatory environment in the spinal cord of ADAM17flox$^{+/+}$-Cx3Cr1-Cre$^{+/-}$ mice correlates to the improved functional recovery observed after SCI.

During SCI, phagocytosis of cellular debris and apoptotic cells by resident microglia and infiltrating monocyte-derived macrophages plays an important role in diminishing inflammation and in initiating repair processes (14). However, the inflammatory M1 or M2 character of these cells is determined by both the type of material they phagocytose and the CNS micro-environment (22). The role of

ADAM17 in shedding various phagocytic receptors gives this enzyme potential in modulating the phagocytic activity of professional phagocytes (24).

The influence of ADAM17 deficiency on the expression of the phagocytic receptors CD36 and TREM2 was determined on gene and/or protein level. ADAM17$^{ex/ex}$ mice show an increased CD36 mRNA expression 7 dpi while CD36 protein expression was increased 28 dpi. Driscoll *et al.* observed an improved phagocytosis of apoptotic cells by macrophage ADAM17 deletion in a model of peritonitis. This effect appears to be mediated by the prevented cleavage and the consequently elevated surface levels of CD36 (33). Besides, ADAM17$^{ex/ex}$ mice also showed higher mRNA levels of the phagocytic receptor TREM2 3 dpi compared to ADAM17$^{wt/wt}$ mice. However, expression of TREM2 at the protein level should be further investigated.

Due to this effect of ADAM17 deficiency on the expression of phagocytic receptors after SCI, it was further investigated whether ADAM17 also influences the *in vitro* phagocytic capacity of BMDMs and primary microglia. Unstimulated and IFN-γ stimulated ADAM17$^{ex/ex}$ BMDMs show a reduce in latex beads phagocytosis while unstimulated and IL-4 stimulated ADAM17$^{ex/ex}$ BMDMs show a higher phagocytic capacity of apoptotic neurons. The discrepancy between phagocytosis of latex beads and apoptotic neurons in ADAM17$^{ex/ex}$ BMDMs could be explained by the different mechanisms in which latex beads and apoptotic neurons are phagocytosed. In contrast to apoptotic neurons, latex beads do not release chemoattractants that trigger phagocyte migration towards their target. Furthermore, latex beads are known to be artificial targets that are usually not taken up by professional phagocytes such as monocyte-derived macrophages via receptor mediated processes (57, 58). On the other hand, LPS stimulated primary microglia show an increased phagocytosis of latex beads. To our knowledge, this is the first study investigating the effect of ADAM17 deficiency on *in vitro* BMDMs and primary microglia phagocytosis of latex beads and apoptotic neurons. Since BMDMs and primary microglia in culture do not mimic the *in vivo* situation in the spinal cord, the effect of ADAM17 deficiency on the *in vivo* phagocytic capacity of professional phagocytes should be further investigated as a next step. One method to evaluate *in vivo* phagocytosis is to determine the number of professional phagocytes that engulfed apoptotic cells using immunofluorescence (59).

Several studies showed the potential beneficial role of phagocytosis after SCI. Boven *et al.* observed that *in vitro* phagocytosis of myelin induces a shift in the expression of pro-inflammatory to anti-inflammatory cytokines (60). This finding was further explored in a study by Kroner *et al.* showing the induction of an *in vitro* M1 to M2 phenotype shift by myelin phagocytosis (34). It is suggested that various pathways, such as inhibition of the nuclear factor-κβ pathway or activation of the peroxisome proliferator-activated receptor β/δ, mediate this phenotypic shift (34, 61). However, it seems that this shift fails to occur in the injured spinal cord. Kroner *et al.* show that the failure of this phenotypic shift is probably due to an increased TNF-α expression in the injured spinal cord during inflammation. Additionally, an increased uptake of intracellular iron from phagocytosed red blood cells or damaged or dying cells by monocyte-derived macrophages and resident microglia also promotes TNF-α expression (14, 34). The impaired shedding of TNF-α in ADAM17$^{ex/ex}$ mice leads to a reduced TNF-α expression in the injured spinal cord. ADAM17 deficiency could therefore be considered as a potential strategy to induce a change in the inflammatory environment of the injured spinal cord after myelin phagocytosis.

5. Conclusion

The goal of this study was to elucidate the effect of ADAM17 on SCI, especially on inflammation and phagocytosis. It was therefore hypothesized that ADAM17 deficiency favors an anti-inflammatory environment by reducing the shedding of inflammatory mediators and by enhancing the resolution of inflammation through phagocytosis leading to an improved functional recovery after SCI. This study provides evidence that ADAM17 and more specifically microglial ADAM17 plays an important role in functional recovery after SCI. Our results suggest that the beneficial effect of ADAM17 deficiency on functional recovery is at least partially mediated by a reduced pro-inflammatory environment in the spinal cord. Furthermore, we also demonstrate that ADAM17 deficiency affects the *in vitro* phagocytic capacity of BMDMs and primary microglia. Future research should focus on investigating the effect of ADAM17 deficiency on the *in vivo* phagocytic capacity of BMDMs and primary microglia.

6. References

1. Dixon TM, Budd MA. Spinal Cord Injury. In: Budd MA, Hough S, Wegener ST, Stiers W, editors. Practical Psychology in Medical Rehabilitation. Cham: Springer International Publishing; 2017. p. 127-36.
2. Varma AK, Das A, Wallace Gt, Barry J, Vertegel AA, Ray SK, et al. Spinal cord injury: a review of current therapy, future treatments, and basic science frontiers. Neurochem Res. 2013;38(5):895-905.
3. Spinal cord injury (SCI): World Health Organization; 2013 [Available from: http://www.who.int/mediacentre/factsheets/fs384/en/.
4. Ahuja CS, Wilson JR, Nori S, Kotter MRN, Druschel C, Curt A, et al. Traumatic spinal cord injury. Nat Rev Dis Primers. 2017;3:17018.
5. Rouanet C, Reges D, Rocha E, Gagliardi V, Silva GS. Traumatic spinal cord injury: current concepts and treatment update. Arq Neuropsiquiatr. 2017;75(6):387-93.
6. McDonald JW, Sadowsky C. Spinal-cord injury. The Lancet. 2002;359(9304):417-25.
7. Oyinbo CA. Secondary injury mechanisms in traumatic spinal cord injury: a nugget of this multiply cascade. Acta Neurobiol Exp (Wars). 2011;71(2):281-99.
8. Zhou X, He X, Ren Y. Function of microglia and macrophages in secondary damage after spinal cord injury. Neural Regeneration Research. 2014;9(20):1787-95.
9. Zhang N, Yin Y, Xu S-J, Wu Y-P, Chen W-S. Inflammation & apoptosis in spinal cord injury. The Indian Journal of Medical Research. 2012;135(3):287-96.
10. Yuan YM, He C. The glial scar in spinal cord injury and repair. Neurosci Bull. 2013;29(4):421-35.
11. Kawano H, Kimura-Kuroda J, Komuta Y, Yoshioka N, Li HP, Kawamura K, et al. Role of the lesion scar in the response to damage and repair of the central nervous system. Cell and Tissue Research. 2012;349(1):169-80.
12. Mueller BK, Mack H, Teusch N. Rho kinase, a promising drug target for neurological disorders. Nat Rev Drug Discov. 2005;4(5):387-98.
13. Donnelly DJ, Popovich PG. Inflammation and its role in neuroprotection, axonal regeneration and functional recovery after spinal cord injury. Experimental neurology. 2008;209(2):378-88.
14. David S, Kroner A. Repertoire of microglial and macrophage responses after spinal cord injury. Nat Rev Neurosci. 2011;12(7):388-99.
15. Neirinckx V, Coste C, Franzen R, Gothot A, Rogister B, Wislet S. Neutrophil contribution to spinal cord injury and repair. J Neuroinflammation. 2014;11:150.
16. Greenhalgh AD, David S. Differences in the Phagocytic Response of Microglia and Peripheral Macrophages after Spinal Cord Injury and Its Effects on Cell Death. The Journal of Neuroscience. 2014;34(18):6316-22.
17. Hines DJ, Hines RM, Mulligan SJ, Macvicar BA. Microglia processes block the spread of damage in the brain and require functional chloride channels. Glia. 2009;57(15):1610-8.
18. Trivedi A, Olivas AD, Noble-Haeusslein LJ. Inflammation and Spinal Cord Injury: Infiltrating Leukocytes as Determinants of Injury and Repair Processes. Clinical neuroscience research. 2006;6(5):283-92.
19. Ishii H, Tanabe S, Ueno M, Kubo T, Kayama H, Serada S, et al. ifn-γ-dependent secretion of IL-10 from Th1 cells and microglia/macrophages contributes to functional recovery after spinal cord injury. Cell Death & Disease. 2013;4(7):e710.
20. Kigerl KA, Gensel JC, Ankeny DP, Alexander JK, Donnelly DJ, Popovich PG. Identification of two distinct macrophage subsets with divergent effects causing either neurotoxicity or regeneration in the injured mouse spinal cord. The Journal of neuroscience : the official journal of the Society for Neuroscience. 2009;29(43):13435-44.
21. Gensel JC, Zhang B. Macrophage activation and its role in repair and pathology after spinal cord injury. Brain Res. 2015;1619:1-11.
22. David S, Greenhalgh AD, Kroner A. Macrophage and microglial plasticity in the injured spinal cord. Neuroscience. 2015;307:311-8.
23. Scheller J, Chalaris A, Garbers C, Rose-John S. ADAM17: a molecular switch to control inflammation and tissue regeneration. Trends Immunol. 2011;32(8):380-7.

24. Zunke F, Rose-John S. The shedding protease ADAM17: Physiology and pathophysiology. Biochim Biophys Acta. 2017.
25. Arribas J, Esselens C. ADAM17 as a therapeutic target in multiple diseases. Curr Pharm Des. 2009;15(20):2319-35.
26. Gooz M. ADAM-17: the enzyme that does it all. Crit Rev Biochem Mol Biol. 2010;45(2):146-69.
27. Moss ML, Minond D. Recent Advances in ADAM17 Research: A Promising Target for Cancer and Inflammation. Mediators of Inflammation. 2017;2017:21.
28. Chalaris A, Adam N, Sina C, Rosenstiel P, Lehmann-Koch J, Schirmacher P, et al. Critical role of the disintegrin metalloprotease ADAM17 for intestinal inflammation and regeneration in mice. J Exp Med. 2010;207(8):1617-24.
29. Blaydon DC, Biancheri P, Di WL, Plagnol V, Cabral RM, Brooke MA, et al. Inflammatory skin and bowel disease linked to ADAM17 deletion. N Engl J Med. 2011;365(16):1502-8.
30. Adrain C, Freeman M. New lives for old: evolution of pseudoenzyme function illustrated by iRhoms. Nat Rev Mol Cell Biol. 2012;13(8):489-98.
31. Cavadas M, Oikonomidi I, Gaspar CJ, Burbridge E, Badenes M, Felix I, et al. Phosphorylation of iRhom2 Controls Stimulated Proteolytic Shedding by the Metalloprotease ADAM17/TACE. Cell Rep. 2017;21(3):745-57.
32. Grieve AG, Xu H, Künzel U, Bambrough P, Sieber B, Freeman M. Phosphorylation of iRhom2 at the plasma membrane controls mammalian TACE-dependent inflammatory and growth factor signalling. eLife. 2017;6:e23968.
33. Driscoll WS, Vaisar T, Tang J, Wilson CL, Raines EW. Macrophage ADAM17 deficiency augments CD36-dependent apoptotic cell uptake and the linked anti-inflammatory phenotype. Circ Res. 2013;113(1):52-61.
34. Kroner A, Greenhalgh Andrew D, Zarruk Juan G, Passos dos Santos R, Gaestel M, David S. TNF and Increased Intracellular Iron Alter Macrophage Polarization to a Detrimental M1 Phenotype in the Injured Spinal Cord. Neuron.83(5):1098-116.
35. Vidal PM, Lemmens E, Avila A, Vangansewinkel T, Chalaris A, Rose-John S, et al. ADAM17 is a survival factor for microglial cells in vitro and in vivo after spinal cord injury in mice. Cell Death Dis. 2013;4:e954.
36. Yona S, Kim K-W, Wolf Y, Mildner A, Varol D, Breker M, et al. Fate mapping reveals origins and dynamics of monocytes and tissue macrophages under homeostasis. Immunity. 2013;38(1):79-91.
37. Nelissen S, Vangansewinkel T, Geurts N, Geboes L, Lemmens E, Vidal PM, et al. Mast cells protect from post-traumatic spinal cord damage in mice by degrading inflammation-associated cytokines via mouse mast cell protease 4. Neurobiol Dis. 2014;62:260-72.
38. Boato F, Hendrix S, Huelsenbeck SC, Hofmann F, Grosse G, Djalali S, et al. C3 peptide enhances recovery from spinal cord injury by improved regenerative growth of descending fiber tracts. J Cell Sci. 2010;123(Pt 10):1652-62.
39. Basso DM, Fisher LC, Anderson AJ, Jakeman LB, McTigue DM, Popovich PG. Basso Mouse Scale for locomotion detects differences in recovery after spinal cord injury in five common mouse strains. J Neurotrauma. 2006;23(5):635-59.
40. Vandesompele J, De Preter K, Pattyn F, Poppe B, Van Roy N, De Paepe A, et al. Accurate normalization of real-time quantitative RT-PCR data by geometric averaging of multiple internal control genes. Genome Biol. 2002;3(7):Research0034.
41. Tamashiro TT, Dalgard CL, Byrnes KR. Primary microglia isolation from mixed glial cell cultures of neonatal rat brain tissue. J Vis Exp. 2012(66):e3814.
42. Yona S, Kim KW, Wolf Y, Mildner A, Varol D, Breker M, et al. Fate mapping reveals origins and dynamics of monocytes and tissue macrophages under homeostasis. Immunity. 2013;38(1):79-91.
43. Wolf Y, Yona S, Kim KW, Jung S. Microglia, seen from the CX3CR1 angle. Front Cell Neurosci. 2013;7:26.
44. Tuszynski MH, Steward O. Concepts and methods for the study of axonal regeneration in the CNS. Neuron. 2012;74(5):777-91.

45. Palazuelos J, Crawford HC, Klingener M, Sun B, Karelis J, Raines EW, et al. TACE/ADAM17 is essential for oligodendrocyte development and CNS myelination. J Neurosci. 2014;34(36):11884-96.
46. Palazuelos J, Klingener M, Raines EW, Crawford HC, Aguirre A. Oligodendrocyte Regeneration and CNS Remyelination Require TACE/ADAM17. J Neurosci. 2015;35(35):12241-7.
47. Ghosh M, Pearse DD. The role of the serotonergic system in locomotor recovery after spinal cord injury. Frontiers in Neural Circuits. 2014;8:151.
48. Bennett ML, Bennett FC, Liddelow SA, Ajami B, Zamanian JL, Fernhoff NB, et al. New tools for studying microglia in the mouse and human CNS. Proceedings of the National Academy of Sciences of the United States of America. 2016;113(12):E1738-E46.
49. Neumann H, Kotter MR, Franklin RJ. Debris clearance by microglia: an essential link between degeneration and regeneration. Brain. 2009;132(Pt 2):288-95.
50. Hendrix S, Kramer P, Pehl D, Warnke K, Boato F, Nelissen S, et al. Mast cells protect from post-traumatic brain inflammation by the mast cell-specific chymase mouse mast cell protease-4. Faseb j. 2013;27(3):920-9.
51. Boato F, Rosenberger K, Nelissen S, Geboes L, Peters EM, Nitsch R, et al. Absence of IL-1beta positively affects neurological outcome, lesion development and axonal plasticity after spinal cord injury. J Neuroinflammation. 2013;10:6.
52. Chu HX, Arumugam TV, Gelderblom M, Magnus T, Drummond GR, Sobey CG. Role of CCR2 in inflammatory conditions of the central nervous system. J Cereb Blood Flow Metab. 2014;34(9):1425-9.
53. Guerrero AR, Uchida K, Nakajima H, Watanabe S, Nakamura M, Johnson WE, et al. Blockade of interleukin-6 signaling inhibits the classic pathway and promotes an alternative pathway of macrophage activation after spinal cord injury in mice. J Neuroinflammation. 2012;9:40.
54. Zhang ZJ, Cao DL, Zhang X, Ji RR, Gao YJ. Chemokine contribution to neuropathic pain: respective induction of CXCL1 and CXCR2 in spinal cord astrocytes and neurons. Pain. 2013;154(10):2185-97.
55. Ruuls SR, Hoek RM, Ngo VN, McNeil T, Lucian LA, Janatpour MJ, et al. Membrane-bound TNF supports secondary lymphoid organ structure but is subservient to secreted TNF in driving autoimmune inflammation. Immunity. 2001;15(4):533-43.
56. Kontoyiannis D, Pasparakis M, Pizarro TT, Cominelli F, Kollias G. Impaired on/off regulation of TNF biosynthesis in mice lacking TNF AU-rich elements: implications for joint and gut-associated immunopathologies. Immunity. 1999;10(3):387-98.
57. Abiega O, Beccari S, Diaz-Aparicio I, Nadjar A, Layé S, Leyrolle Q, et al. Neuronal Hyperactivity Disturbs ATP Microgradients, Impairs Microglial Motility, and Reduces Phagocytic Receptor Expression Triggering Apoptosis/Microglial Phagocytosis Uncoupling. PLOS Biology. 2016;14(5):e1002466.
58. Park D, Han CZ, Elliott MR, Kinchen JM, Trampont PC, Das S, et al. Continued clearance of apoptotic cells critically depends on the phagocyte Ucp2 protein. Nature. 2011;477:220.
59. Sierra A, Encinas JM, Deudero JJ, Chancey JH, Enikolopov G, Overstreet-Wadiche LS, et al. Microglia shape adult hippocampal neurogenesis through apoptosis-coupled phagocytosis. Cell Stem Cell. 2010;7(4):483-95.
60. Boven LA, Van Meurs M, Van Zwam M, Wierenga-Wolf A, Hintzen RQ, Boot RG, et al. Myelin-laden macrophages are anti-inflammatory, consistent with foam cells in multiple sclerosis. Brain. 2006;129(Pt 2):517-26.
61. Bogie JF, Jorissen W, Mailleux J, Nijland PG, Zelcer N, Vanmierlo T, et al. Myelin alters the inflammatory phenotype of macrophages by activating PPARs. Acta Neuropathol Commun. 2013;1:43.

7. Supplemental information

7.1. Materials and methods

Table S1: Primers used for genotyping.

	Primer sequence (5' to 3')
ADAM17$^{wt/ex}$	Forward = TATGTGATAGGTGTAATG Reverse = CTTATTATTCTCGTGGTCACC
ADAM17flox$^{+/+}$	Common = TGGGGAAGCAAAGTTGTAGG Wildtype Reverse = TCTCTGGACCCCTTCTTCCT Mutant Reverse = CTTCGTATAATGTATGCTATACG
Cx3Cr1-Cre$^{+/-}$	Forward = GGTTCGCAAGAACCTGATGGACAT Reverse = GCTAGAGCCTGTTTTGCACGTTCA

Table S2: Forward and reverse primers used for qPCR.

	Forward primer (5' to 3')	**Reverse primer (5' to 3')**
HMBS	GATGGGCAACTGTACCTGACTG	CTGGGCTCCTCTTGGAATG
GAPDH	GGCCTTCCGTGTTCCTAC	TGTCATCATATCTGGCAGGTT
ADAM17	AGAGAGCCATCTGAAGAGTTTGT	CTTCTCCACGGCCCATGTAT
TNF-α	GTCCCCAAAGGGATGAGAAGT	TTTGCTACGACGTGGGCTAC
IL-1β	ACCCTGCAGCTGGAGAGTGT	TTGACTTCTATCTTGTTGAAGACAAACC
IL-6	TGTCTATACCACTTCACAAGTCGGAG	GCACAACTCTTTTCTCATTTCCAC
CXCL1	GCCTATCGCCAATGAGCTG	CTGAACCAAGGGAGCTTCAGG
CCR2	CAGGTGACAGAGACTCTTGGAATG	GAACTTCTCTCCAACAAAGGCATAA
TREM2	ATGGGACCTCTCCACCAGTT	TCACGTACCTCCGGGTCCA
CD36	GGACATTGAGATTCTTTTCCTCTG	GCAAAGGCATTGGCTGGAAGAAC

Table S3: Primary and secondary antibodies used for western blot.

	Primary antibody	**Secondary antibody** (1/2000) (Dako)
ADAM17	rabbit α-ADAM17 (1/2000) (Abcam)	goat α-rabbit
Arg-1	mouse α-Arginase-1 (1/1000) (Santa Cruz Biotechnologies, Heidelberg, Germany)	rabbit α-mouse
CD36	rabbit α-CD36 (1/1000) (Abcam)	goat α-rabbit
β-actin	mouse α-β-actin (1/5000) (Santa Cruz Biotechnologies)	rabbit α-mouse

Table S4: Primary and secondary antibodies used for immunohistochemistry.

	Primary antibody	**Secondary antibody** (Invitrogen)
GFAP	mouse α-GFAP (1/500) (Sigma-Aldrich)	goat α-mouse Alexa 568 (1/250)
MBP	rat α-MBP (1/250) (Merck Millipore)	goat α-rat Alexa 488 (1/250)
Iba-1	rabbit α-Iba-1 (1/350) (Wako, Neuss, Germany)	goat α-rabbit Alexa 488 (1/250)
	goat α-Iba-1 (1/250) (Novus Biologicals, Abingdon, United Kingdom)	donkey α-goat Alexa 488 (1/400)
CD4	rat α-CD4 (1/250) (BD Biosciences)	goat α-rat Alexa 568 (1/250)
Arg-1	mouse α-Arginase-1 (1/100) (Santa Cruz Biotechnology)	goat α-mouse Alexa 568 (1/400)
MHC-II	rat α-MHC-II (1/200) (Santa Cruz Biotechnology)	goat α-rat Alexa 488 (1/400)
5-HT	rabbit α-5-HT (1/1000) (ImmunoStar, Kampenhout, Belgium)	donkey α-rabbit Alexa 555 (1/250)
TMEM119	rabbit α-TMEM119 (1/100) (Abcam)	donkey α-rabbit Alexa 555 (1/400)

7.2. Results

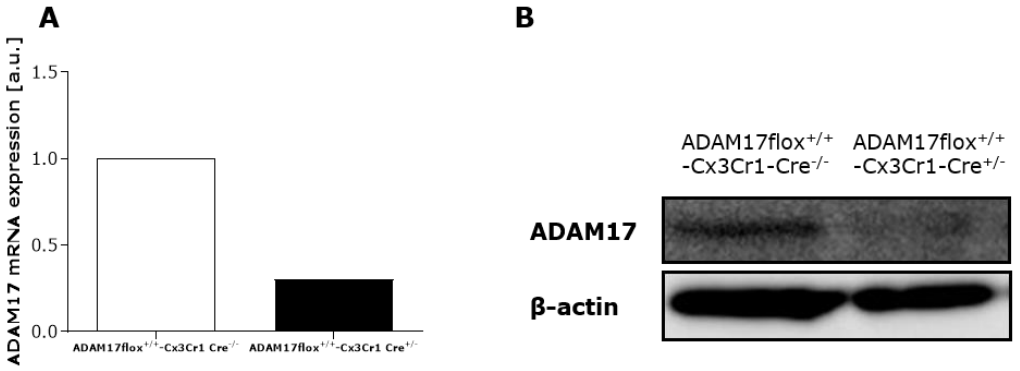

Figure S1: Efficient Cre-lox recombination in microglia. The efficiency of Cre-lox recombination was determined by measuring ADAM17 expression at the gene level by qPCR (A) and at the protein level (98 kDA) by western blot (B). A-B) Both qPCR and western blot analysis showed an efficient Cre-lox recombination in microglia. A = Relative quantification of gene expression levels was performed by the comparative $2^{-\Delta\Delta CT}$ method. Data were normalized to the most stable reference genes HMBS and GAPDH. B = β-actin (42 kDA) is used as a loading control. *ADAM17, 'a disintegrin and metalloproteinase 17'; qPCR, quantitative polymerase chain reaction; HMBS, hydroxymethylbilane synthase; GAPDH, glyceraldehyde 3-phosphate dehydrogenase.*

Auteursrechtelijke overeenkomst

Ik/wij verlenen het wereldwijde auteursrecht voor de ingediende eindverhandeling:
Microglia-specific ADAM17 deficiency improves functional recovery after spinal cord injury

Richting: **Master of Biomedical Sciences-Clinical Molecular Sciences**
Jaar: **2018**

in alle mogelijke mediaformaten, - bestaande en in de toekomst te ontwikkelen - , aan de Universiteit Hasselt.

Niet tegenstaand deze toekenning van het auteursrecht aan de Universiteit Hasselt behoud ik als auteur het recht om de eindverhandeling, - in zijn geheel of gedeeltelijk -, vrij te reproduceren, (her)publiceren of distribueren zonder de toelating te moeten verkrijgen van de Universiteit Hasselt.

Ik bevestig dat de eindverhandeling mijn origineel werk is, en dat ik het recht heb om de rechten te verlenen die in deze overeenkomst worden beschreven. Ik verklaar tevens dat de eindverhandeling, naar mijn weten, het auteursrecht van anderen niet overtreedt.

Ik verklaar tevens dat ik voor het materiaal in de eindverhandeling dat beschermd wordt door het auteursrecht, de nodige toelatingen heb verkregen zodat ik deze ook aan de Universiteit Hasselt kan overdragen en dat dit duidelijk in de tekst en inhoud van de eindverhandeling werd genotificeerd.

Universiteit Hasselt zal mij als auteur(s) van de eindverhandeling identificeren en zal geen wijzigingen aanbrengen aan de eindverhandeling, uitgezonderd deze toegelaten door deze overeenkomst.

Voor akkoord,

Corstjens, Inge

Datum: **7/06/2018**